1962

# Energy transfer properties of thin magnetic film logical elements

Terry Allen Smay
*Iowa State University*

# ENERGY TRANSFER PROPERTIES OF THIN MAGNETIC FILM LOGICAL ELEMENTS

by

Terry Allen Smay

A Dissertation Submitted to the

Graduate Faculty in Partial Fulfillment of

The Requirements for the Degree of

DOCTOR OF PHILOSOPHY

Major Subject: Electrical Engineering

Approved:

Signature was redacted for privacy.

In Charge of Major Work

Signature was redacted for privacy.

Head of Major Department

Signature was redacted for privacy.

Dean of Graduate College

Iowa State University
Of Science and Technology
Ames, Iowa

1962

TABLE OF CONTENTS

# I. INTRODUCTION

The thin magnetic film with uniaxial anisotropy has been for several years the subject of intensive research in regard to its application in various types of electronic devices. A wide range of rather diverse applications including balanced modulators (18, 20), parametric amplifiers (18, 19), and parametrons (14, 18, 21) have been investigated but by far the most intensive work has gone into the use of such an element as a simple switching element in digital computer storage and logical systems. Memory applications are most numerous (1, 2, 13, 15, 16, 17), although promising applications to computer logic (7, 9) have also been proposed.

Several small film memories are now commercially available and skepticism regarding the feasibility of large film memories seems to be diminishing. Before such memories are possible on a large-scale basis, however, not only must the problems associated with the film characteristics be solved, but a clearer understanding of the behavior of the film element as determined by the characteristics of the coupling lines must be obtained. It is the purpose of this dissertation to examine this latter problem. A brief analysis of the general problem is given by Eggenberger (6), but the brevity of this analysis leaves many questions unanswered, and, at least as far as one important point is concerned, the results presented there are in rather direct conflict with those presented in the analysis contained herein.

The analysis given here will consist of a rather detailed examination of the switching behavior of a magnetic film as it is influenced by its associated coupling lines. Most systems proposed so far use one of two

types of bit gemoetry:

1. Two-wire drive and sense strip lines enclose a single planar film element. This geometry has two primary disadvantages. First, the single planar film has, for small bits, a large demagnetizing field. Second, substrate thickness may prohibit tight magnetic coupling to the lines.
2. The film is deposited on a polished metallic substrate and single drive and sense strip lines are laid over the film. Coupling is improved, but the demagnetizing field problem still exists and image currents flowing in the metallic substrate ground plane may contribute a detrimental d-c field if repetition rate is high.

The type of geometry to be examined here is illustrated in Figure 1. Rather than sandwiching one film between two-wire lines, two films sandwich single lines, the two exterior ground planes forming the return path. This geometry has several advantages. First, if the films are closely spaced, an essentially closed flux path is provided, reducing the demagnetizing field problem. Second, since essentially all flux passes from film edge to film edge, little flux penetrates the ground planes, so that nearly all eddy-current loss occurs in the center lines which may be made very thin. Third, a three-conductor strip line of this type not only reduces radiation problems because of the ground-plane shielding, but also minimizes the image-current problem described above under 2, since any symmetrical current components flowing in the two ground planes tend to produce fields which cancel near the center of the line where the films are. Fourth, the substrate thickness does not limit the coupling of film flux to the central

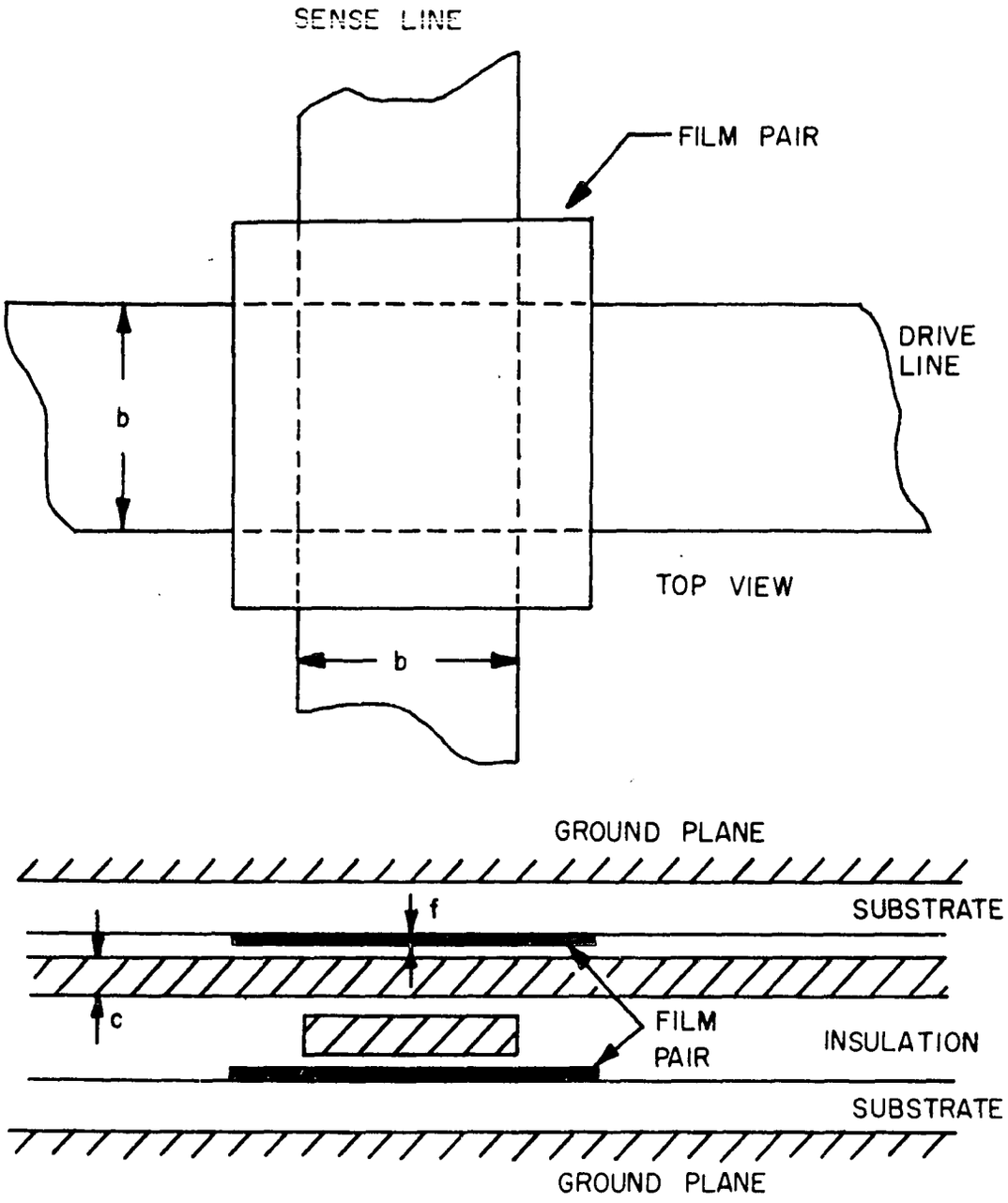


**Figure 1. Coupled-pair geometry**

lines. Thick substrates do, however, increase the characteristic impedance of the line, necessitating higher drive energy for a given drive field.

In order to simplify calculations, both drive and sense lines are assumed to have a width of b meters. Also, no separate "write" or "word" line to provide a restoring field is included, it being assumed that the sense line may also perform this function. The analysis to follow is not invalidated by violation of these conditions, but some simplification is achieved and, practically speaking, the assumed conditions may indeed be quite appropriate in a particular application.

It may be noted that, in Figure 1, the film itself is somewhat larger than the common area of the crossed lines. However, if the films are placed quite close to the lines, drive and restore fields will have sufficient magnitude to cause magnetization rotation in only this smaller region, resulting in an effective film size equal to about this common area. Therefore, in the analysis to follow, the effective film size will be assumed to be b meters by b meters. The spacing between films is d meters, drive and sense line thicknesses are c meters, and film thickness is f meters.

## II. ENERGY TRANSFER ANALYSIS

The basic problem to be considered is as follows: For a given drive-line current and corresponding drive field, how much energy is coupled into the sense line? Strictly speaking, it is not just the amount of energy that is desired, but the speed of delivery and the voltage waveform, these quantities implicitly giving the energy if the sense-line characteristic impedance is known. It is these quantities that will therefore be sought in the analysis. The several fields which influence film switching are as follows:

1. The drive field produced by the drive-line current. This is a known quantity and will be assumed to be a step function, i.e., to have a zero rise time.
2. The shielding field which seeks to keep the normal component of magnetic flux density at a conductor surface constant when the applied magnetic flux density has time variation. This is an inductive effect which implies no energy loss, since it will tend to restore the magnetization to its remanent state if the drive field is removed.
3. The eddy-current field which results from the electric field induced in the conductor when the conductor is pierced by a time-varying magnetic flux density. This field is proportional to the time rate of change of the flux density, and is therefore a resistive effect, representing energy loss.
4. The back-emf field resulting from current induced in the drive line by the time rate of change of the magnetic film flux linkages

about this line. If the line characteristic impedance properly contains the effect of the film inductance, this field is included in the drive field and is negligible in any event.

5. The sense-line field resulting from current induced in the sense line. Since the sense-line impedance will be at least a few ohms and since the equivalent eddy-current resistance representing 3 above is a small fraction of an ohm, as the analysis will show, this field represents much less energy loss than the eddy-current field and is therefore negligible.

## A. Relaxation Time Analysis

In order to ascertain the effect of the shielding field it is necessary to know over what time interval it is effective, i.e., it is necessary to know its "L/R time constant". A simplified model will be used to determine this quantity. Consider the strip line whose cross-sectional end view is shown in Figure 2. If a remotely generated magnetic field of magnitude $B_o$ is applied as a step function in the direction shown, the z-direction fields are as shown in Figure 2(a). A flux density in the y-direction will also be present in order to preserve continuity of $\underline{B}$, but this is not shown. Since no flux may exist within the conductor at time $t = 0$, the component of magnetic flux density produced by the conductor within the conductor is $B_o$ in the positive z-direction, as shown in Figure 2(b). Within the conductor, by Maxwell's equations neglecting displacement current,

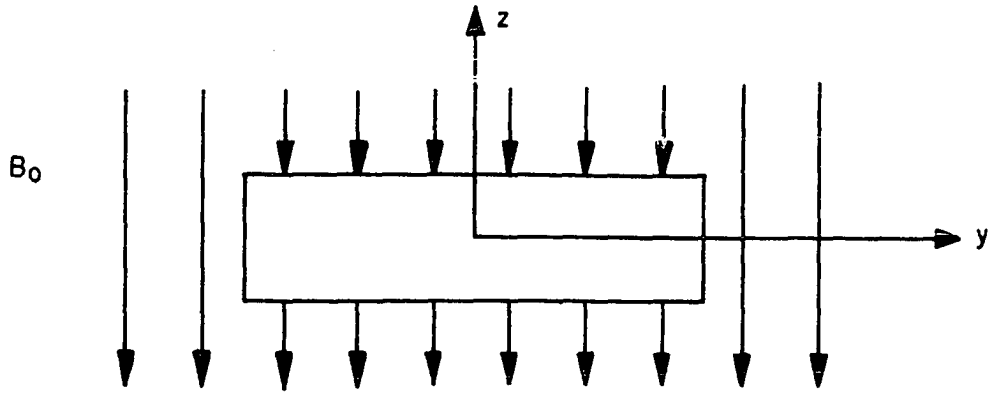


(a) INITIAL FIELDS IN z DIRECTION.

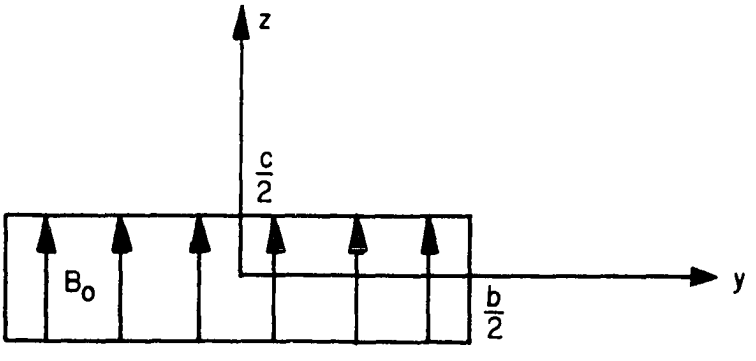


(b) INITIAL FIELDS WITHIN THE CONDUCTOR PRODUCED BY THE CONDUCTOR.

**Figure 2. Model for calculation of penetration time**

$$\nabla \times \underline{\mathcal{E}} = \nabla \times \left(\frac{\nabla \times \underline{H}}{\sigma}\right) = \frac{1}{\sigma}\left[\nabla\left(\nabla \cdot \underline{H}\right) - \nabla^2 \underline{H}\right]$$

$$= -\frac{1}{\sigma}\nabla^2 \underline{H} = -\frac{1}{\mu\sigma}\nabla^2 \underline{B} = -\frac{\partial \underline{B}}{\partial t}$$

$$\nabla^2 \underline{B} = \mu\sigma \frac{\partial \underline{B}}{\partial t} \tag{1}$$

Within the conductor, $B_x = 0$, $\partial/\partial x = 0$, so the equation for $B_z$ reduces to

$$\frac{\partial^2 B_z}{\partial y^2} + \frac{\partial^2 B_z}{\partial z^2} = \mu\sigma \frac{\partial B_z}{\partial t} \tag{2}$$

Outside the conductor, $\sigma = 0$, so, once again neglecting displacement current,

$$\frac{\partial^2 B_z}{\partial y^2} + \frac{\partial^2 B_z}{\partial z^2} = 0 \tag{3}$$

These components of $\underline{B}$ are those contributed by the presence of the conductor and do not include the applied field $-\underline{a}_z B_o$. The initial condition on Equation 2 is:

$$B_z\,(y,\ z,\ 0) = B_o \tag{4}$$

Two solutions to this problem will be considered, one for $c \gg b$, the other for $b \gg c$, i.e., one with the applied flux tangential to the strip line, the other with the applied flux normal to the strip line.

1. Applied flux tangential to strip line

If $c \gg b$, the initial flux distribution runs parallel to the long dimension of the strip line. Two boundary conditions on Equation 2 are

$$B_z\,(-\,b/2,\ z,\ t) = 0$$

$$B_z\,(b/2,\ z,\ t) = 0 \qquad (5)$$

The boundary conditions at $z = \pm\, c/2$ are more complex because of continuity requirements at these surfaces, but since $c \gg b$, the flux pattern relaxes almost entirely in the lateral direction, so that only variations in the y direction need be considered. The validity of this statement will be more apparent after completion of the next section.

If z variations may be neglected, the solution to Equation 2 and boundary conditions given by Equations 4 and 5 obtained by separation of the variables may be written as

$$B_z(y,\ t) = \frac{4B_o}{\pi} \sum_m \frac{1}{m} \operatorname{Sin} \frac{m\pi}{2} \operatorname{Cos} \frac{m\pi y}{b} \exp\left(-\frac{m^2\pi^2 t}{b^2 \mu\, \sigma}\right) \qquad (6)$$

The time constant of longest duration is that for m = 1, and it is given by

$$\tau_{max} = \frac{b^2 \mu \sigma}{\pi^2} \qquad (7)$$

For copper 1/2 mil thick, $\tau_{max}$ is

$$\tau_{max} = 1.19 \text{ nanoseconds} \qquad (8)$$

This time constant is valid for applied fields tangential to the stripline surface. In the physical situation under consideration, such a field is the drive-line field as applied to the sense line (see Figure 1). Thus, for 1/2 mil copper lines, the drive field should essentially penetrate the sense line and be applied to both films after about 2 nanoseconds.

2. Applied flux normal to strip line

If $b \gg c$, the initial flux distribution within the conductor is normal to the strip-line top and bottom surfaces. The solution to Equation 2 is considerably more complex in this case, since simple boundary conditions such as those given by Equations 5 do not apply. A rigorous solution would consist of finding a solution to Equation 2 within the conductor and matching it at the boundary to a solution of Equation 3 outside the conductor. Such a solution is quite complex and will not be attempted here. Rather, since the dominant time constant is determined, as in the previous case, by the lowest order component of $B_z$, a one-term solution to Equation 2 will be postulated and matched to a one-term solution of Equation 3. Such solutions will not match the initial condition given by Equation 4, but should permit a good determination of the dominant time constant of the system. A solution to Equation 2 valid within the conductor is:

$$B_z(y, z, t) = A \cos \frac{\pi y}{b} \cos \frac{\pi z}{c'} \exp \left(- \frac{\beta^2}{\mu\sigma} t \right) \qquad (9)$$

where:

$$\beta^2 = \left(\frac{\pi}{b}\right)^2 + \left(\frac{\pi}{c'}\right)^2 \qquad (10)$$

A is an arbitrary constant, and c' is a fundamental interval on z greater than c and the value of which must be determined. Such an interval permits continuity of $B_z$ at the conductor surface. The solution to Equation 3 is quite complex at large distances from the conductor because of the cylindrical boundary conditions, but, for z slightly greater than c/2 it may

be approximated by:

$$B_z = C \cos \frac{\pi y}{b} \exp\left(-\frac{\pi z}{b}\right) \exp\left(-\frac{\beta^2}{\mu\sigma} t\right) \tag{11}$$

where C is an arbitrary constant. Equation 3 does not fix the exponential time behavior given in Equation 11, but it must be of the same form as that of Equation 9 if solution matching is to be effected.

At $z = c/2$, both solutions must be equal because of continuity. This leads to

$$A \cos \frac{\pi c}{2c'} = C \exp\left(-\frac{\pi c}{2b}\right) \tag{12}$$

Also, at $y = 0$, $c/2 = z$, an application of the divergence equation $\nabla \cdot B = 0$ shows that:

$$\left.\frac{\partial B_z}{\partial z}\right|_{z = c/2 -} = \left.\frac{\partial B_z}{\partial z}\right|_{z = c/2 +} \tag{13}$$

This leads to the relationship

$$\left(\frac{\pi}{c'}\right) A \sin \frac{\pi c}{2c'} = \left(\frac{\pi}{b}\right) C \exp\left(-\frac{\pi c}{2b}\right) \tag{14}$$

Division of Equation 14 by Equation 12 results in

$$\tan \frac{\pi c}{2c'} = \frac{c'}{b} \tag{15}$$

This transcendental equation has no general solution, but, assuming $c'/b \ll 1$,

$$\frac{\pi}{2}\frac{c}{c'} \approx \frac{c'}{b}$$

or

$$c' = \sqrt{\frac{\pi}{2} bc} \tag{16}$$

so that c' is approximately the geometric mean of b and c, and since $b \gg c$, the original assumption is justified. Using this value of c', Equations 9 and 10 yield

$$\tau_{max} = \frac{\mu\sigma}{\beta^2} = \frac{\mu \sigma}{\frac{\pi^2}{b^2} + \frac{2\pi}{bc}} = \frac{bc\mu\sigma}{2\pi} \tag{17}$$

For b = 10 mils, c = 1/2 mil, Equation 17 yields

$$\tau_{max} = 37.4 \text{ nanoseconds} \tag{18}$$

Thus the time constant for flux normally penetrating a thin conductor is much greater than that for flux tangentially penetrating a conductor of the same thickness. This means that even though the strip lines are thin enough to permit the drive field to quickly penetrate the sense line and drive both films, the flux coupling the two films, which attempts to penetrate the conductors normally, may not do so, but may instead "wrap around" the conductors.

In concluding the analysis of inductive relaxation effects, it should be emphasized that only the z components of magnetic flux density have been considered. The other components could possibly have been found by further application of Maxwell's equations, and other solutions valid outside the conductor could also be determined so as to obtain better understanding of

the way in which the flux lines "wrap around" the conductor until penetration is effected, but the complexity of such further analysis and the marginal value of information obtained by such analysis for the problem at hand makes the prospect rather unattractive, and it will not be done here.

Now that the effect of conductor geometry on inductive relaxation time is known, the switching field analysis will be performed. Because the general problem is quite complex, the two limiting cases of zero relaxation time and infinite relaxation time will be analyzed separately. Relaxation time here refers to that corresponding to normal flux penetration. An intelligent prediction of the performance of a physical logical element should then be possible since the previous relaxation-time analysis should permit judgment as to which of the two cases is most indicative of the physical situation.

### B. Case 1 - Zero Relaxation Time

In this case the time-varying flux coupling the two magnetic films is assumed to penetrate the thin strip lines instantaneously, inducing eddy currents which in turn cause resistive losses in the conductors, this energy loss evidencing itself as torque applied to the film magnetization $\underline{M}$. The first step in performing the analysis is to examine the nature of the actual flux distribution penetrating the conductors. Since zero relaxation time is assumed, slowly-varying fields are implied, and static field analysis will give this distribution.

Refer to Figure 3. The flux piercing the conductor, assumed to lie midway between films, emanates from the four film edges perpendicular to

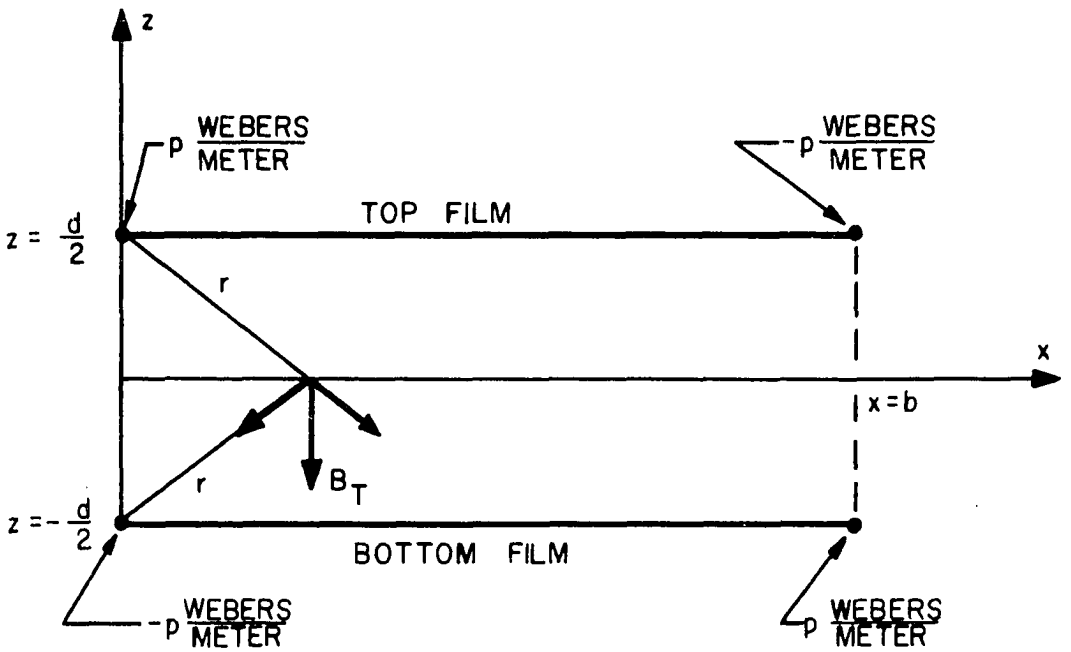


Figure 3. Line pole model for calculation of flux density

the plane of the paper if single-domain films are assumed. These edges will be approximated by infinitely long line magnetic poles, each having a pole strength of p webers/unit length, as indicated. p will depend on the component of magnetization $\underline{M}$ perpendicular to the film edge and on the film thickness f. This infinite-line approximation is in fact quite good for close film spacings, the error occuring at the near and far conductor edges, the conductor being b meters in width and running in the x direction. The line pole approximation represents an idealization, of course, since in actuality the flux will emanate from a distribution of free poles in the vicinity of the film edges. Both these idealizations will tend to cause calculated energy loss to exceed actual energy loss.

At an arbitrary point x along the center line shown in Figure 3, the normal flux density $B_T$ is given by

$$B_T = \frac{p}{2\pi r} \cdot \frac{d}{2r} + \frac{p}{2\pi r} \cdot \frac{d}{2r}$$

$$= \frac{p\,d}{2\pi r^2} = \frac{p\quad d}{2\pi[x^2 + (\frac{d}{2})^2]} \qquad (19)$$

This calculation has included the contribution of only the one pair of infinite lines at x = 0, but for any reasonably close film spacing the other pair make an extremely negligible contribution to the flux density. Appendix A gives the exact expression including all four lines and also gives the total flux coupled between adjacent poles. It is shown that, for b/d greater than about 5, at least 90 per cent of the flux emanating from a given pole closes on its adjacent neighbor, substantiating earlier remarks concerning the ability of the coupled pair to minimize

demagnetizing field effects and eddy current losses in the exterior ground planes.

The functional form given in Equation 19 is not a particularly convenient one for use. It will therefore be approximated by the form shown in Figure 4 along with that given by Equation 19. This approximation is

$$B_T = \begin{cases} \frac{2p}{a} \cos^2 \frac{\pi x}{a} & |x| < \frac{a}{2} \\ 0 & |x| > \frac{a}{2} \end{cases} \qquad (20)$$

At $x = 0$, both form should have the same peak value, implying that

$$a = \pi d \qquad (21)$$

Note that the integral over all x of the function given by Equation 20 is equal to p, which says that the total flux represented is equal to that emanating from the top line pole and closing on the bottom line pole, a logical result.

The net result is that the flux distribution assumed to exist because of the proximity of adjacent film edges to a centrally located thin conductor is that given by Equation 20.

The eddy-current analysis will now be performed on the following basis: The flux distribution given by Equation 20, centered at $x = 0$, will be considered to be applied normally to a thin conductor, as shown in Figure 5. Region 1 is the region in which the flux is applied, Region 2 is the region where no flux is applied. Maxwell's equations will be used to calculate the current densities resulting from this distribution, these densities will be squared and interpreted in terms of power loss, and this loss will be used to describe the damping field affecting film switching.

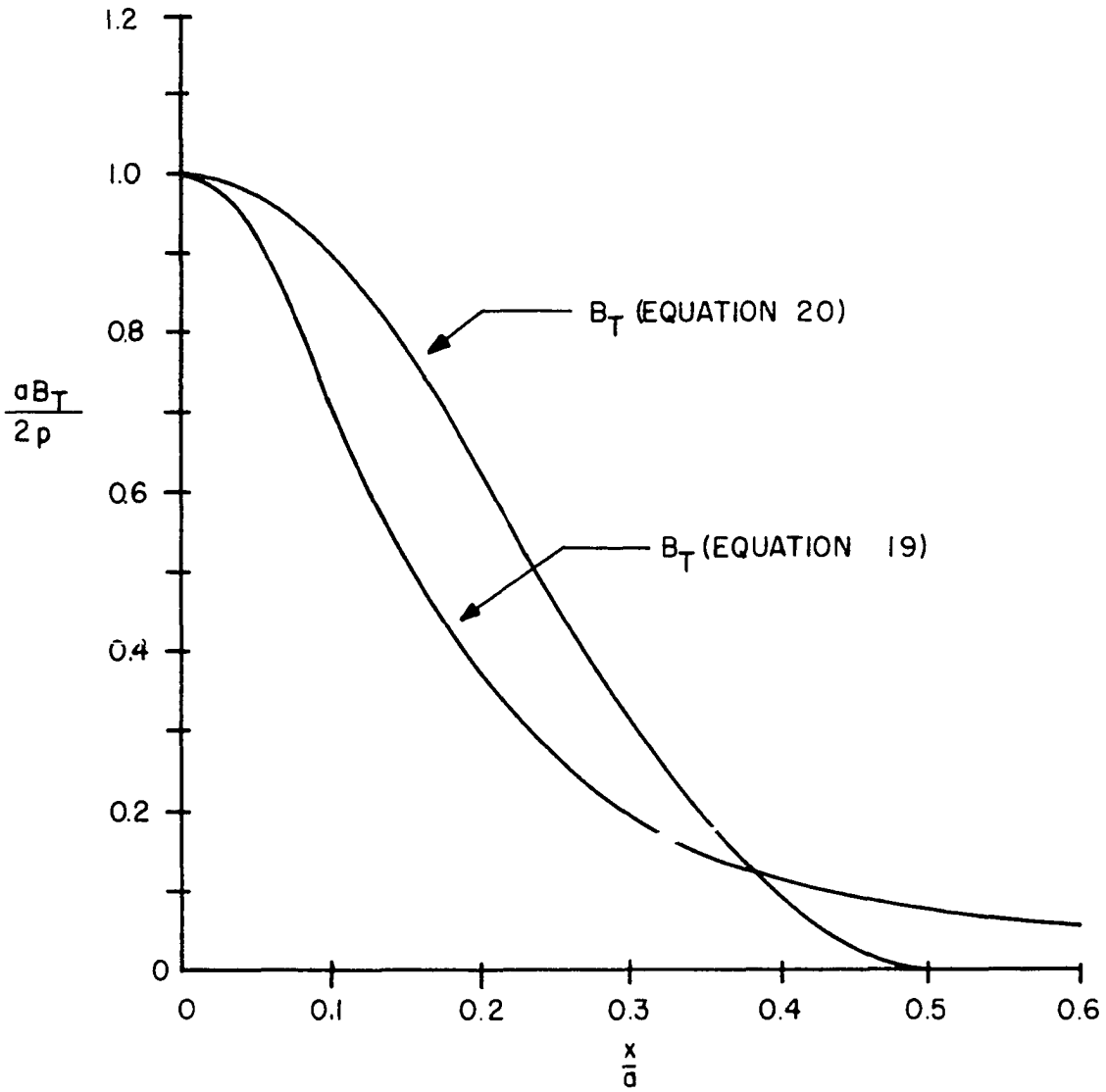


Figure 4. Normalized flux density between coupled film pair

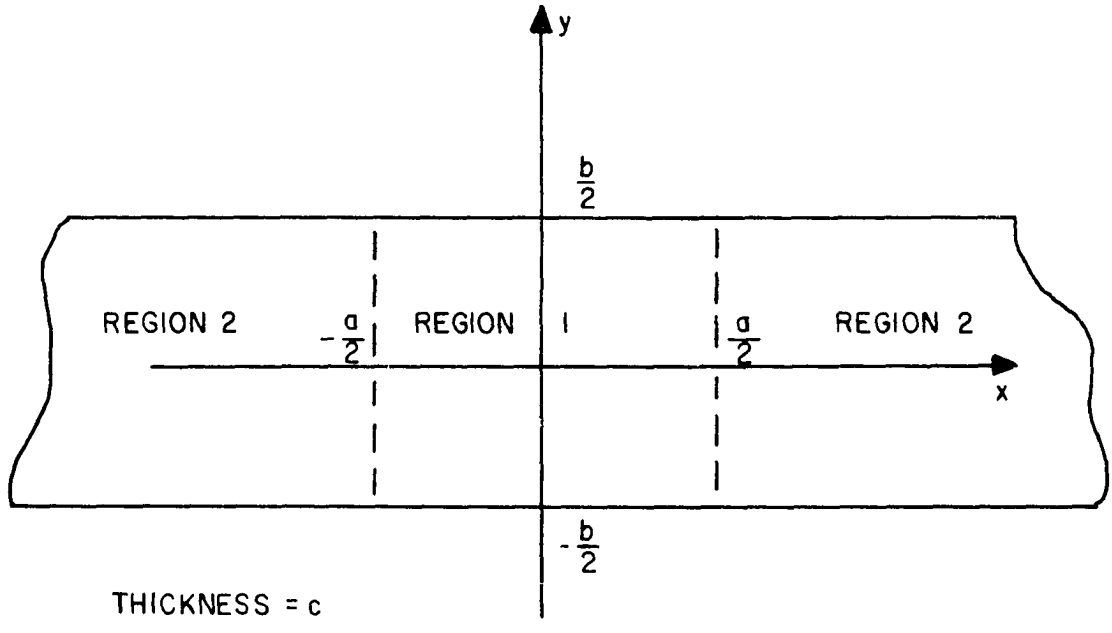


Figure 5. Strip-line model for eddy-current calculations

The appropriate equations to be solved are

$$\nabla^2 \underline{i} = 0 \tag{22}$$

$$\nabla \times \underline{i} = -\sigma \frac{\partial \underline{B}}{\partial t} \tag{23}$$

where $\underline{i}$ is the vector current density, in amperes/square meter. Since only resistive effects are being considered, it is permissible to assume a particular type of time variation of the applied field, namely

$$B_T(x, t) = \left[\frac{2p}{a\Delta T} \cos^2 \frac{\pi x}{a}\right] t = B_o(x)t \tag{24}$$

where $p/\Delta T$ is a constant time rate of change of the linear pole density. This particular form for $B_T$ implies a "constant-voltage" drive and the resulting eddy-current distribution, as would be expected, is constant with time. This is not a restrictive assumption, since, if resistive effects predominate, the equivalent eddy-current resistance found for this type of drive field may be used to find instantaneous power loss for an arbitrary time variation of $B_T$.

Assuming $B_T$ to be applied in the positive z direction, Equations 22 and 23 become

$$\begin{aligned}
\frac{\partial^2 i_x}{\partial x^2} + \frac{\partial^2 i_x}{\partial y^2} + \frac{\partial^2 i_x}{\partial z^2} &= 0 \\
\frac{\partial^2 i_y}{\partial x^2} + \frac{\partial^2 i_y}{\partial y^2} + \frac{\partial^2 i_y}{\partial z^2} &= 0 \\
\frac{\partial^2 i_z}{\partial x^2} + \frac{\partial^2 i_z}{\partial y^2} + \frac{\partial^2 i_z}{\partial z^2} &= 0
\end{aligned} \tag{25}$$

$$\frac{\partial i_z}{\partial y} = \frac{\partial i_y}{\partial z}$$

$$\frac{\partial i_x}{\partial z} = \frac{\partial i_z}{\partial x}$$

$$\frac{\partial i_y}{\partial x} - \frac{\partial i_x}{\partial y} = \begin{cases} -\sigma B_o(x) & \text{, Region 1} \\ 0 & \text{, Region 2} \end{cases} \qquad (26)$$

1. Current distribution in Region 1

A general solution to Equations 25 in Region 1, using appropriate boundary conditions, is

$$i_x = \sum_m \sum_n A_{mn} \operatorname{Sin} \frac{m\pi y}{b} \operatorname{Cos} \frac{n\pi z}{c} \operatorname{Cosh} \beta x$$

$$i_y = \sum_m \sum_n B_{mn} \operatorname{Cos} \frac{m\pi y}{b} \operatorname{Cos} \frac{n\pi z}{c} \operatorname{Sinh} \beta x$$

$$i_z = \sum_m \sum_n C_{mn} \operatorname{Sin} \frac{m\pi y}{b} \operatorname{Sin} \frac{n\pi z}{c} \operatorname{Sinh} \beta x \qquad (27)$$

where

$$\beta = \left(\frac{m\pi}{b}\right)^2 + \left(\frac{n\pi}{c}\right)^2$$

This solution may be broken up as follows:

$$i_x = \sum_m A_{mo} \operatorname{Sin} \frac{m\pi y}{b} \operatorname{Cosh} \frac{m\pi x}{b} + \sum_m \sum_{n>o} A_{mn} \operatorname{Sin} \frac{m\pi y}{b} \operatorname{Cos} \frac{n\pi z}{c} \operatorname{Cosh} \beta x$$

$$i_y = \sum_m B_{mo} \operatorname{Cos} \frac{m\pi y}{b} \operatorname{Sinh} \frac{m\pi x}{b} + \sum_m \sum_{n>o} B_{mn} \operatorname{Cos} \frac{n\pi z}{c} \operatorname{Cos} \frac{m\pi y}{b} \operatorname{Sinh} \beta x$$

$$i_z = 0 + \sum_m \sum_{n>o} C_{mn} \operatorname{Sin} \frac{m\pi y}{b} \operatorname{Sin} \frac{n\pi z}{c} \operatorname{Sinh} \beta x \qquad (28)$$

For very thin conductors, intuition tells us that $i_z$ will approach zero, as will variations with z, i.e., x and y currents will approach uniformity across the cross-section as c goes to zero. This means that the double series in Equations 28 will become negligibly small for small c and a good approximation to the actual current distribution is given by only the left-hand terms of Equations 28. It must be noted, however, that this is an approximation, since in the presence of a time-varying $B_x$, as is the case for the physical situation under examination, by the curl equation,

$$\frac{\partial i_z}{\partial y} - \frac{\partial i_y}{\partial z} = - \sigma \frac{\partial B_x}{\partial t} \qquad (29)$$

This means that, although $B_x$ and $\partial B_x/\partial t$ become very small for very thin conductors, they are not zero, which in turn means that $i_z$ and variations with z are also not zero. The reason for emphasizing this approximation is that some difficulties are encountered in applying the current continuity equation if this is not kept in mind. An alternative integral form of the continuity equation will be used to circumvent this difficulty.

Applying $\nabla \cdot \underline{i} = 0$, the current continuity equation, to the exact general solution given by Equations 27 results in

$$A_{mo} = B_{mo} \equiv A_m \tag{30}$$

Now using the approximate solution described above and combining it with the curl Equation 26, the solution to Equations 25 and 26 (remembering that the thin-conductor approximation causes violation of current continuity at some boundaries) is

$$\begin{aligned} i_{x1} &= \sum_m A_m \operatorname{Sin} \frac{m\pi y}{b} \operatorname{Cosh} \frac{m\pi x}{b} + k_1 \sigma B_o(x) y \\ i_{y1} &= \sum_m A_m \operatorname{Cos} \frac{m\pi y}{b} \operatorname{Sinh} \frac{m\pi x}{b} - k_2 \sigma \int_o^x B_o(x)dx \end{aligned} \tag{31}$$

where $k_1$ and $k_2$ are arbitrary constants and the 1 subscripts indicate currents in Region 1. One relationship between $k_1$ and $k_2$ may be found by reapplying the curl of Equation 26, resulting in

$$\frac{\partial i_{y1}}{\partial x} - \frac{\partial i_{x1}}{\partial y} = - \sigma B_o(x)$$

$$- k_2 \sigma B_o(x) - k_1 \sigma B_o(x) = - \sigma B_o(x) \tag{32}$$

$$k_1 + k_2 = 1$$

2. Current distribution in Region 2

For positive x, the fact that the current densities must go to zero as x goes to infinity results in a solution of the form

$$\begin{aligned} i_{x2} &= \sum_m B_m \operatorname{Sin} \frac{m\pi y}{b} \exp\left(- \frac{m\pi x}{b}\right) \\ i_{y2} &= \sum_m -B_m \operatorname{Cos} \frac{m\pi y}{b} \exp\left(- \frac{m\pi x}{b}\right) \end{aligned} \tag{33}$$

The fact that the Fourier coefficients are equal in magnitude and opposite

in sign results once again from application of the current continuity equation. Since no applied field exists in Region 2 none of the previous problems regarding setting $i_z$ equal to zero occur here.

3. Matching boundary conditions between Region 1 and Region 2

Evaluation of the constants $A_m$ and $B_m$ may be accomplished by noting that, at $x = a/2$, the boundary between Region 1 and Region 2, both $i_x$ and $i_y$ must be continuous, the first because the normal component of current flowing across the boundary must be continuous, the second because an integration of electric field about a path slightly within Region 1 encloses the same flux as an integration about a path slightly outside Region 1, implying continuity of electric field tangential to $x = a/2$ and consequently implying continuity of $i_y$. Employing these conditions results in

$$\sum_m A_m \text{Sin} \frac{m\pi y}{b} \text{Cosh} \frac{m\pi a}{2b} + k_1 \sigma B_o \left(\frac{a}{2}\right) y = \sum_m B_m \text{Sin} \frac{m\pi y}{b} \exp\left(-\frac{m\pi a}{2b}\right)$$

$$\sum_m A_m \text{Cos} \frac{m\pi y}{b} \text{Sinh} \frac{m\pi a}{2b} - k_2 \sigma \int_o^{\frac{a}{2}} B_o(x)dx =$$

$$\sum_m -B_m \text{Cos} \frac{m\pi y}{b} \exp\left(-\frac{m\pi a}{2b}\right) \qquad (34)$$

Rearranging gives

$$k_1 \sigma B_o(\tfrac{a}{2}) y = \sum_m [-A_m \text{Cosh } \tfrac{m\pi a}{2b} + B_m \exp(-\tfrac{m\pi a}{2b})] \text{ Sin } \tfrac{m\pi y}{b} =$$

$$\sum_m C_m \text{Sin } \tfrac{m\pi y}{b}$$

$$k_2 \sigma \int_o^{\frac{a}{2}} B_o(x)dx = \sum_m [A_m \text{Sinh } \tfrac{m\pi a}{2b} + B_m \exp(-\tfrac{m\pi a}{2b})] \text{ Cos } \tfrac{m\pi y}{b} = \tag{35}$$

$$\sum_m D_m \text{Cos } \tfrac{m\pi y}{b}$$

Equation 20 indicates that $B_o(a/2) = 0$, implying $C_m = 0$. Define

$$K_a \equiv \int_o^{\frac{a}{2}} B_o(x)dx \tag{36}$$

which says that

$$k_2 \sigma K_a = \sum_m D_m \text{ Cos } \tfrac{m\pi y}{b}, \quad |y| < \tfrac{b}{2} \tag{37}$$

This means that the $D_m$'s are just Fourier cosine square wave coefficients, given by

$$D_m = \frac{4k_2 \sigma K_a}{m \pi} \text{ Sin } \tfrac{m\pi}{2} \tag{38}$$

Equations 35 then yield the relationships

$$\begin{aligned} -A_m \text{Cosh } \tfrac{m\pi a}{2b} + B_m \exp(-\tfrac{m\pi a}{2b}) &= 0 \\ A_m \text{Sinh } \tfrac{m\pi a}{2b} + B_m \exp(-\tfrac{m\pi a}{2b}) &= \frac{4k_2 \sigma K_a}{m \pi} \text{ Sin } \tfrac{m\pi}{2} \end{aligned} \tag{39}$$

The solution to these equations is

$$A_m = \frac{4k_2\,\sigma\,K_a\,\exp\left(-\frac{m\pi a}{2b}\right)}{m\,\pi}\,\mathrm{Sin}\,\frac{m\pi}{2}$$

$$B_m = \frac{4k_2\,\sigma\,K_a}{m\,\pi}\,\mathrm{Cosh}\,\frac{m\pi a}{2b}\,\mathrm{Sin}\,\frac{m\pi}{2} \qquad (40)$$

The final solution for the current densities is

$$i_{x1} = \frac{4k_2\,\sigma\,K_a}{\pi}\sum_m \frac{1}{m}\exp\left(-\frac{m\pi a}{2b}\right)\mathrm{Sin}\,\frac{m\pi}{2}\,\mathrm{Sin}\,\frac{m\pi y}{b}\,\mathrm{Cosh}\,\frac{m\pi x}{b} + k_1\sigma B_o(x)y$$

$$i_{y1} = \frac{4k_2\sigma K_a}{\pi}\sum_m \frac{1}{m}\exp\left(-\frac{m\pi a}{2b}\right)\mathrm{Sin}\,\frac{m\pi}{2}\,\mathrm{Cos}\,\frac{m\pi y}{b}\,\mathrm{Sinh}\,\frac{m\pi x}{b} - k_2\sigma\int_o^x B_o(x)dx$$

$$i_{x2} = \frac{4k_2\sigma K_a}{\pi}\sum_m \frac{1}{m}\,\mathrm{Cosh}\,\frac{m\pi a}{2b}\,\mathrm{Sin}\,\frac{m\pi}{2}\,\mathrm{Sin}\,\frac{m\pi y}{b}\exp\left(-\frac{m\pi x}{b}\right)$$

$$i_{y2} = \frac{4k_2\sigma K_a}{\pi}\sum_m -\frac{1}{m}\,\mathrm{Cosh}\,\frac{m\pi a}{2b}\,\mathrm{Sin}\,\frac{m\pi}{2}\,\mathrm{Cos}\,\frac{m\pi y}{b}\exp\left(-\frac{m\pi x}{b}\right) \qquad (41)$$

$k_1$ and $k_2$ remain to be evaluated. This may be done by noting that the total x-direction current flowing across the half-plane given by $x = 0$, $y > 0$, is equal to the negative of the y-direction current flowing across the half-plane given by $y = 0$, $x > 0$. This relationship is used in Appendix B with the result

$$k_1 = 0.702\left(\frac{a}{b}\right)^2 k_2 \qquad (42)$$

which, when combined with Equation 32 yields

$$k_1 = \frac{0.702}{(b/a)^2 + 0.702}$$

$$k_2 = \frac{(b/a)^2}{(b/a)^2 + 0.702} \qquad (43)$$

4. Power calculations

Now that the current densities throughout the conducting region between a pair of film edges are known, it is possible to find the power dissipation represented by these current densities. The appropriate expression for power dissipated within a conducting volume V of conductivity $\sigma$ is

$$P = \frac{1}{\sigma} \iiint_V [i_x^2 + i_y^2 + i_z^2] \, dv \tag{44}$$

In this case, since $i_z$ is assumed to be negligibly small, implying uniformity of $i_x$ and $i_y$ in the z direction, the expression becomes

$$P = \frac{8c}{\sigma} \int_0^{\frac{a}{2}} \int_0^{\frac{b}{2}} (i_{x1}^2 + i_{x2}^2) dy dx + \int_{\frac{a}{2}}^{\infty} \int_0^{\frac{b}{2}} (i_{x2}^2 + i_{y2}^2) dy dx \tag{45}$$

The factor of eight occurs because the volume considered represents one-eighth of the power loss, remembering that there are two pairs of film edges causing eddy currents in the line. It has been assumed that the two pairs of film edges are remote enough so that negligible overlapping of eddy-current patterns occurs. The first term within the brackets in Equation 45 represents power loss in Region 1 and the second term power loss in Region 2.

Evaluation of the integrals in Equation 45 is a matter of straightforward, if tedious, integration. Some benefit is gained by integrating with respect to y first, since the orthogonality of the sine and cosine functions in Equation 45 over the interval $0 < y < b/2$ eliminates many

undesirable cross-products. When the integration is accomplished, the result is

$$P = \frac{16k_2^2\sigma K_a^2 b^2 c}{\pi^3}\sum_m \frac{1+\exp(-\frac{m\pi a}{b})}{m^3}\ \mathrm{Sin}^2\frac{m\pi}{2}$$

$$+\frac{64k_1k_2\sigma K_a b^2 c}{\pi^2}\sum_m \frac{\exp(-\frac{m\pi a}{2b})}{m^2}\ \mathrm{Sin}\frac{m\pi}{2}\left(\frac{1}{2}+\frac{1}{m\pi}\mathrm{Sin}\frac{m\pi}{2}\right)\int_o^{\frac{a}{2}} B_o(x)\cdot \mathrm{Cosh}\frac{m\pi x}{b}\,dx$$

$$-\frac{64k_2^2\sigma K_a bc}{\pi^2}\sum_m \frac{\exp(-\frac{m\pi a}{2b})}{m^2}\ \mathrm{Sin}^2\frac{m\pi}{2}\int_o^{\frac{a}{2}} K_{2x}\ \mathrm{Sinh}\frac{m\pi x}{b}\,dx$$

$$+4k_2^2\sigma bc\int_o^{\frac{a}{2}} k_{2x}^2\,dx+\frac{1}{3}k_1^2\sigma b^3 c\int_o^{\frac{a}{2}}[B_o(x)]^2dx \qquad (46)$$

where

$$k_{2x}\equiv\int_o^x B_o(x)dx \qquad (47)$$

If $B_o(x)$ as given by Equation 24 is inserted into Equation 46, the result is, after simplification,

$$P = \left(\frac{pb}{\Delta T}\right)^2 (4\sigma c k_2) \left\{ \frac{k_2}{\pi^3} \sum_m \frac{1 + \exp\left(-\frac{m\pi a}{b}\right)}{m^3} \operatorname{Sin}^2 \frac{m\pi}{2} \right.$$

$$+ \frac{16k_1(b/a)^3}{\pi^3} \sum_m \frac{\operatorname{Sin} \frac{m\pi}{2}\left(\frac{1}{2} + \frac{1}{m\pi} \operatorname{Sin} \frac{m\pi}{2}\right)}{m^3 \left[4(b/a)^2 + m^2\right]} \left[1 - \exp\left(-\frac{m\pi a}{b}\right)\right]$$

$$- \frac{4k_2(b/a)}{\pi^3} \sum_m \frac{\operatorname{Sin}^2 \frac{m\pi}{2}}{m^3} \left[ \frac{1 + \exp\left(-\frac{m\pi a}{b}\right)}{2(b/a)} - \frac{4\left(\frac{b}{a}\right)^2 - 4\left(\frac{b}{a}\right)^2 \exp\left(-\frac{m\pi a}{b}\right)}{m\pi \left[m^2 + 4\left(\frac{b}{a}\right)^2\right]} \right]$$

$$\left. + \frac{0.0733k_2}{\frac{b}{a}} + \frac{0.0625k_1^2\left(\frac{b}{a}\right)}{k_2} \right\} \qquad (48)$$

The quantity $(pb/\Delta T)$ is the constant time rate of change of the total magnetic flux emanating from one of the film edges and may therefore be considered to be the "driving voltage" $e_f$ supplying the eddy-current power loss. This leads to

$$P = \frac{(pb/\Delta T)^2}{R_e} = \frac{e_f^2}{R_e} \qquad (49)$$

or

$$R_e = \frac{(pb/\Delta T)^2}{P} \qquad (50)$$

where $R_e$ is the equivalent eddy-current resistance seen by the film driving voltage $e_f$ and is implicitly given by Equation 48. Note that $R_e$ is a function of only the conductor thickness c and the ratio b/a, since $k_1$ and $k_2$ are also functions of this ratio (Equations 43). $cR_e$ is plotted in Figure 6 for copper conductors as a function of b/a.

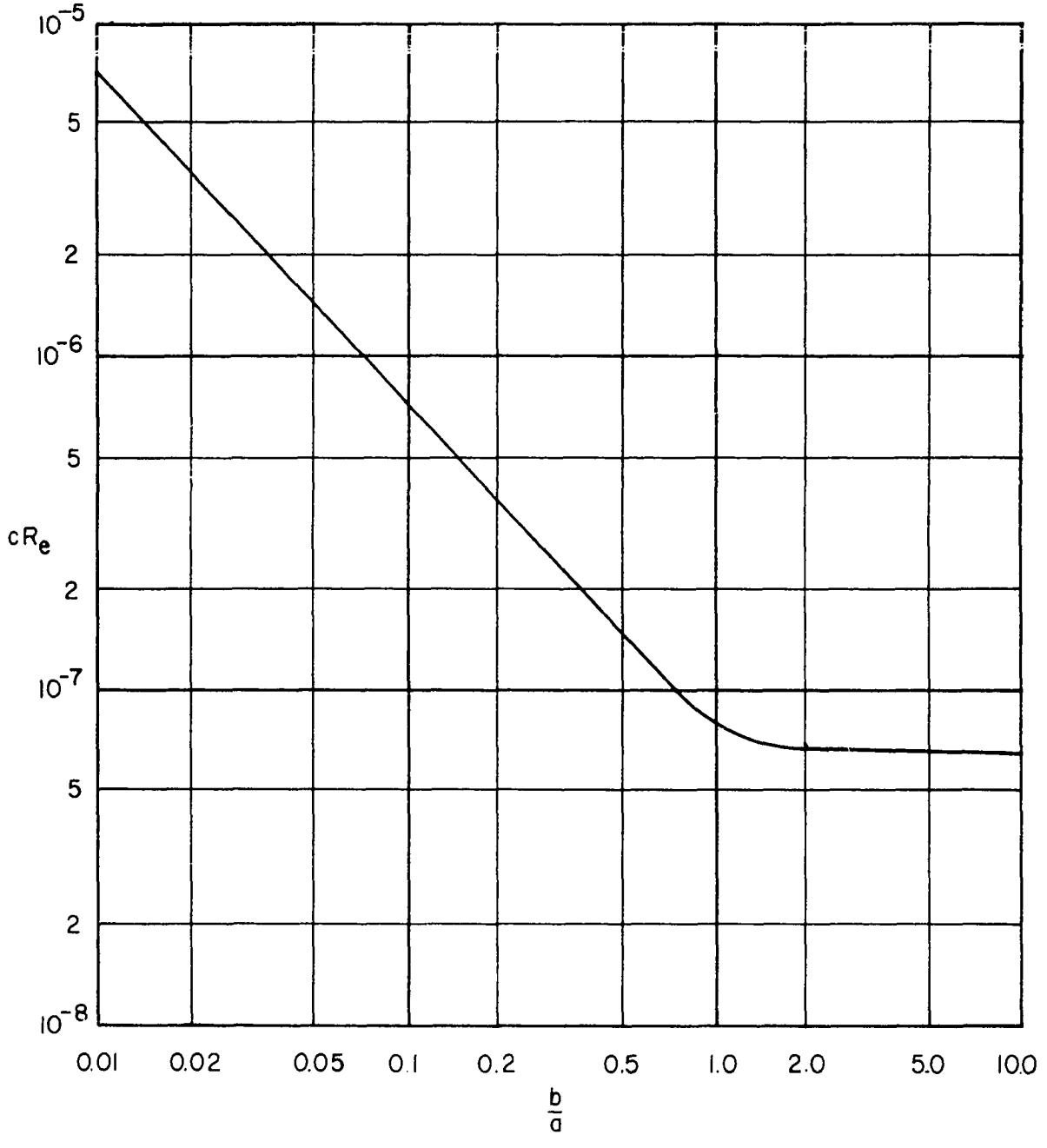


Figure 6. Equivalent eddy-current resistance of strip line

## 5. Switching time calculations

In the previous section a means for obtaining eddy-current power loss in a strip line passing between the film pair was found under the assumption of zero inductive relaxation time. This work will now be applied in analyzing the effect of such losses on film switching. The following conditions are assumed to be true:

1. The particular switching mode to be examined is that where the easy direction of magnetization of the film is perpendicular to the drive field, i.e., the film is driven in the hard direction, causing the magnetization vector to be rotated 90 degrees for sufficiently high drive fields. This particular mode lends itself well to calculation and experimentation, and the results obtained are subject to extension in analyzing other switching modes. Note that, in this mode, the easy direction of magnetization is parallel to the drive line and longitudinal restore pulses may be applied by passing currents through the sense line.
2. Homogeneous single-domain rotational switching is assumed. This is justifiable for small films, since even though eddy-current fields are not uniformly applied over the film volume, exchange forces and demagnetizing fields will cause the film to maintain its single-domain structure, effectively distributing the torque over the entire film volume.
3. The viscous-flow approximation, as described by Smith (22) and Olson and Pohm (12) will be used to describe the dynamic behavior of the film magnetization. The error encountered in using this

approximation comes about because of partially neglecting magnetization precession out of the plane of the film, but the time of this precession is somewhat less than total switching time, so the error should not be great.

The linear pole density representing the divergence of magnetization at the film edges perpendicular to the drive line is (see Figure 1)

$$p_d = Mf \text{ Cos } \theta \tag{51}$$

and that representing the divergence of magnetization of the edges over the sense line is

$$p_s = Mf \text{ Sin } \theta \tag{52}$$

where $\theta$ is the angle the magnetization makes with the easy direction in the plane of the film, and M is the magnitude of the magnetization vector. Differentiating with respect to time we obtain

$$\frac{dp_d}{dt} = -Mf \text{ Sin } \theta \dot{\theta}$$

$$\frac{dp_s}{dt} = Mf \text{ Cos } \theta \dot{\theta} \tag{53}$$

These time derivatives may now be used to replace $p/\Delta T$ in Equation 49 to describe total eddy-current loss in both lines, resulting in

$$P = \frac{(Mf \text{ b } \dot{\theta})^2}{R_e} (\text{Sin}^2 \theta + \text{Cos}^2 \theta)$$

$$= \frac{(Mf \text{ b } \dot{\theta})^2}{R_e} \tag{54}$$

This power loss evidences itself as a torque $\underline{T}_e$ applied to the magnetization vector $\underline{M}$. The assumption of homogeneous rotation allows us to consider this torque to be an average torque applied over the entire film volume.

$$T_e \dot{\theta} = \text{power loss per unit film volume}$$

$$= \frac{P}{2b^2 f} = \frac{M^2 f \dot{\theta}^2}{2R_e}$$

$$T_e = \frac{M^2 f}{2R_e} \dot{\theta} \tag{55}$$

Since this torque is directly proportional to $\dot{\theta}$ it is indeed a viscous damping torque and may be described in terms of a dimensionless damping constant $\alpha_e$ in the following way:

$$T_e = \frac{M^2 f}{2R_e} \dot{\theta} = \frac{\alpha_e M}{\gamma} \dot{\theta}$$

$$\alpha_e = \frac{\gamma M f}{2R_e} \tag{56}$$

where $\gamma$ is the magnitude of the gyromagnetic ratio (about $2.21 \times 10^5$ cycles per second per ampere per meter for 80-20 Permalloy). The reason for defining $\alpha_e$ this way is to give a comparison with the phenomenological damping constant $\alpha$ commonly encountered in working with the Landau-Lifshitz (11) and Gilbert (8) equations, as described by Smith (22) and Olson and Pohm (12). In the viscous-flow approximation, this damping torque is the major factor inhibiting switching and may be set equal to the drive torque caused by the drive field. The effective drive torque $T_d$, which includes the effect of the uniaxial anisotropy, may be found by consideration of

the free energy E of the film, given by:

$$E = K_1 \sin^2 \theta - H_d M \sin \theta \tag{57}$$

where $K_1$ is a constant describing the uniaxial anisotropy of the film and $H_d$ is the magnitude of the drive field. The effective drive torque may now be found by differentiating this function with respect to $\theta$.

$$T_d(\theta) = \frac{dE}{d\theta} = 2K_1 \sin \theta \cos \theta - H_d M \cos \theta$$

$$= H_k M \cos \theta \left(\sin \theta - \frac{H_d}{H_k}\right) \tag{58}$$

where $H_k \equiv 2K_1/M$, and is called the anisotropy field. The anisotropy field causes a torque in the same sense as the viscous damping torque for positive $\dot{\theta}$, i.e., both tend to oppose the rotation of the magnetization vector toward $\theta = 90^\circ$. Summing torques in the proper sense,

$$T_e + T_d = 0$$

$$\frac{\alpha_e M}{\gamma} \dot{\theta} + H_k M \cos \theta \left(\sin \theta - \frac{H_d}{H_k}\right) = 0$$

$$\dot{\theta} = \frac{\gamma H_k}{\alpha_e} \cos \theta \left(\frac{H_d}{H_k} - \sin \theta\right) \tag{59}$$

The time elapsed between application of the drive field and magnetization rotation to any arbitrary angle $\theta_1$ is thus

$$t = \frac{\alpha_e}{\gamma H_k} \int_0^{\theta_1} \frac{d\theta}{\cos \theta \left(\frac{H_d}{H_k} - \sin \theta\right)} = \frac{\alpha_e M}{\gamma} \int_0^{\theta_1} \frac{d\theta}{-T_d(\theta)} \tag{60}$$

The flux linking the sense line is that flux emanating from the film edges

perpendicular to the drive line and is given by

$$\phi_s = Mf\ b\ \text{Cos}\ \theta \tag{61}$$

The sense line voltage is thus

$$e_s = \frac{d\phi_s}{dt} = Mf\ b\ \text{Sin}\ \theta\ \dot{\theta}$$

$$= \frac{fbr}{\alpha_e}\ T_d(\theta)\ \text{Sin}\ \theta \tag{62}$$

by Equations 58 and 59. In order to evaluate this voltage as a function of time it is necessary to solve Equation 60 to obtain $\theta$ as a function of time and then to use Equation 62 to find $e_s$ as a function of $\theta$. Figure 7 shows $-T_d/MH_k$ plotted as a function of $\theta$ for various drive fields. Rather laborious numerical integration was performed to obtain solutions to Equation 60 from the curves of Figure 7 and then to calculate $e_s$ from Equation 62. The results of these calculations are shown in Figure 8. The very long tail on the voltages occurs because, as $\theta$ approaches 90 degrees, the drive torque and with it the sense line voltage approaches zero.

This analysis gives the sense-line voltage for the limiting case of zero inductive relaxation time for the shielding fields. The analysis to follow will indicate the type of switching to be expected in the other limiting case, i.e., when the inductive relaxation time is infinite.

### C. Case 2 - Infinite Relaxation Time

If the flux penetration time constant as given in Equation 17 is very long with respect to the film switching time, the flux pattern within the conductor is not permitted to change appreciably during film switching.

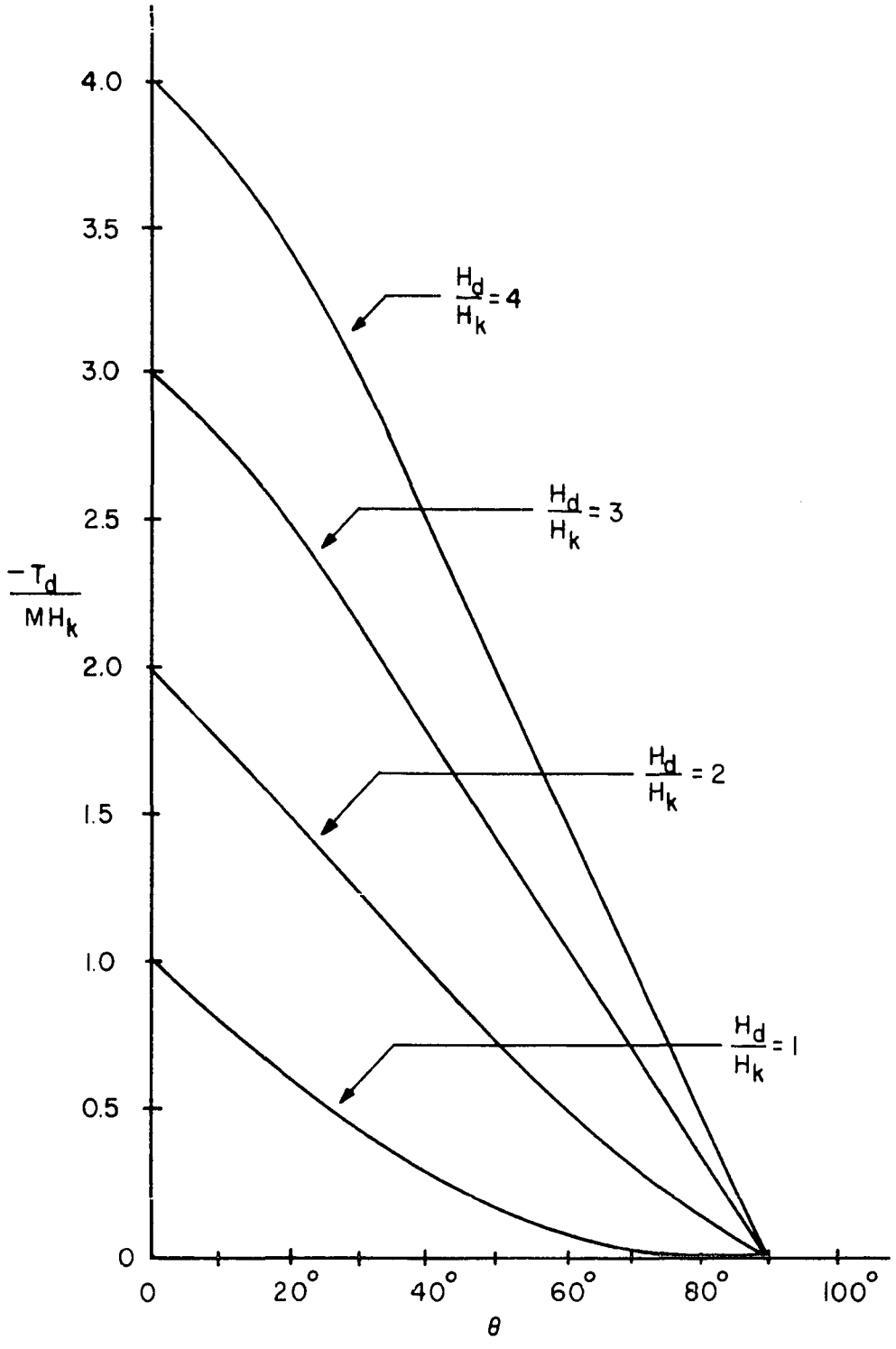


Figure 7. Normalized effective driving torque versus θ

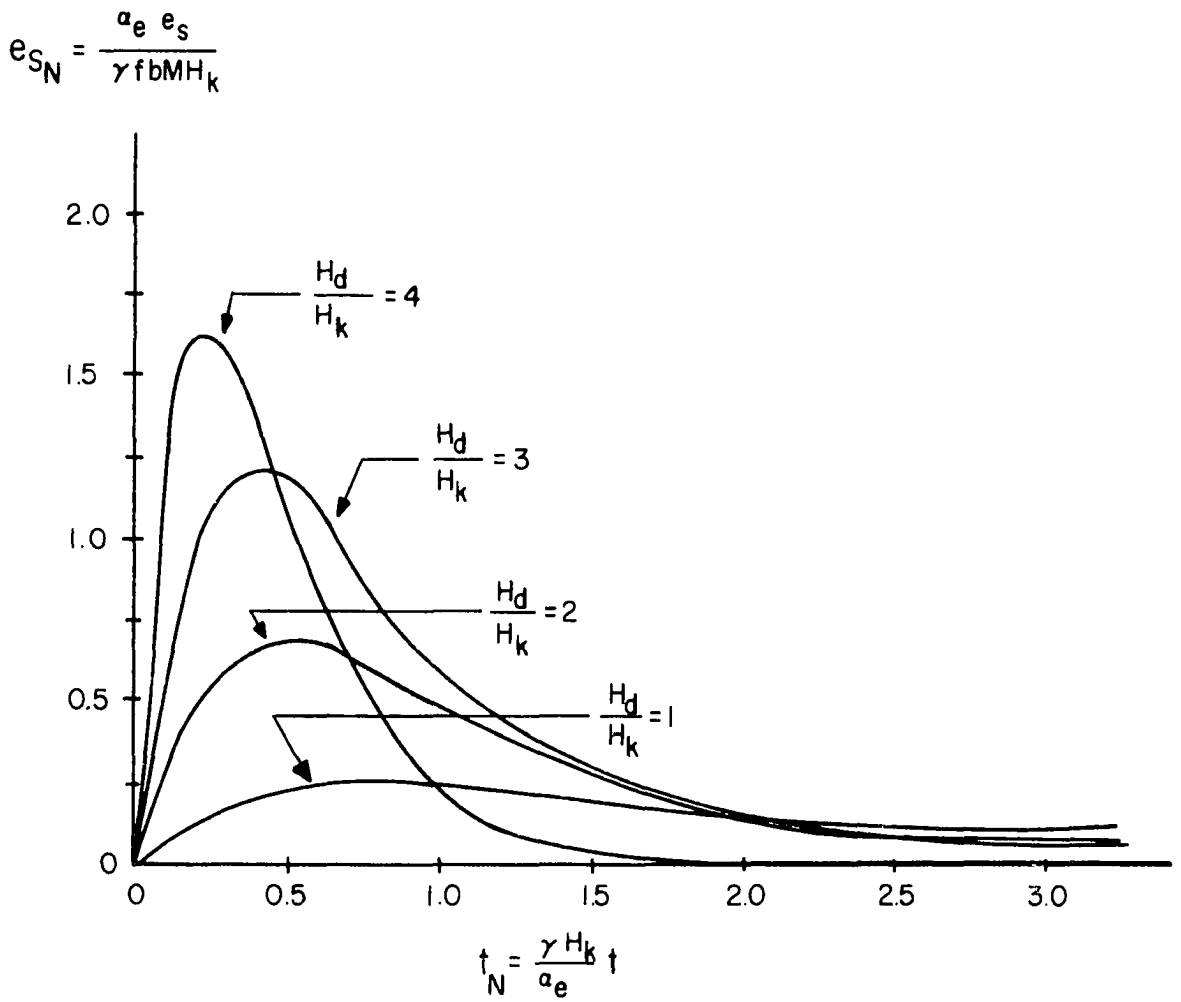


Figure 8. Normalized sense-line voltage versus normalized time

In other words, the flux penetrating the conductor before application of the drive field is "trapped" during switching, while any flux lines the film attempts to force through the conductor are repelled at the conductor surface. It is important to note that fields affecting film switching caused by this effect do not represent energy loss, since if the drive field is suddenly terminated, these fields tend to restore the magnetization to its original state, returning the stored energy to the system.

An attempt will be made here to calculate approximately the effects of such "trapped-flux" fields on film switching. The method will be as follows: the presence of the conductor will be considered to contribute the same effect as if a variable source of magnetic flux were positioned under each of the film edges at the conductor surface. The flux density produced by these sources will be such as to satisfy the proper boundary condition at the conductor surface, i.e., to maintain the normal component of flux density at the same value as it was before magnetization rotation began.

The first step is to determine the flux density each of these sources should have. Figure 4 gives the infinite line pole flux distribution calculated from Equation 19. Since only rough estimates are desired from this portion of the analysis, a cruder approximation than that given in Figure 4 will be used here. The actual flux distribution given by Figure 4 will be represented by a uniform distribution 2d in width centered at the plane connecting film edges, as shown in Figure 9. Only one film is considered. The film considered to be in a remanent state and the flux emanating from the film edge is considered to penetrate the copper in a

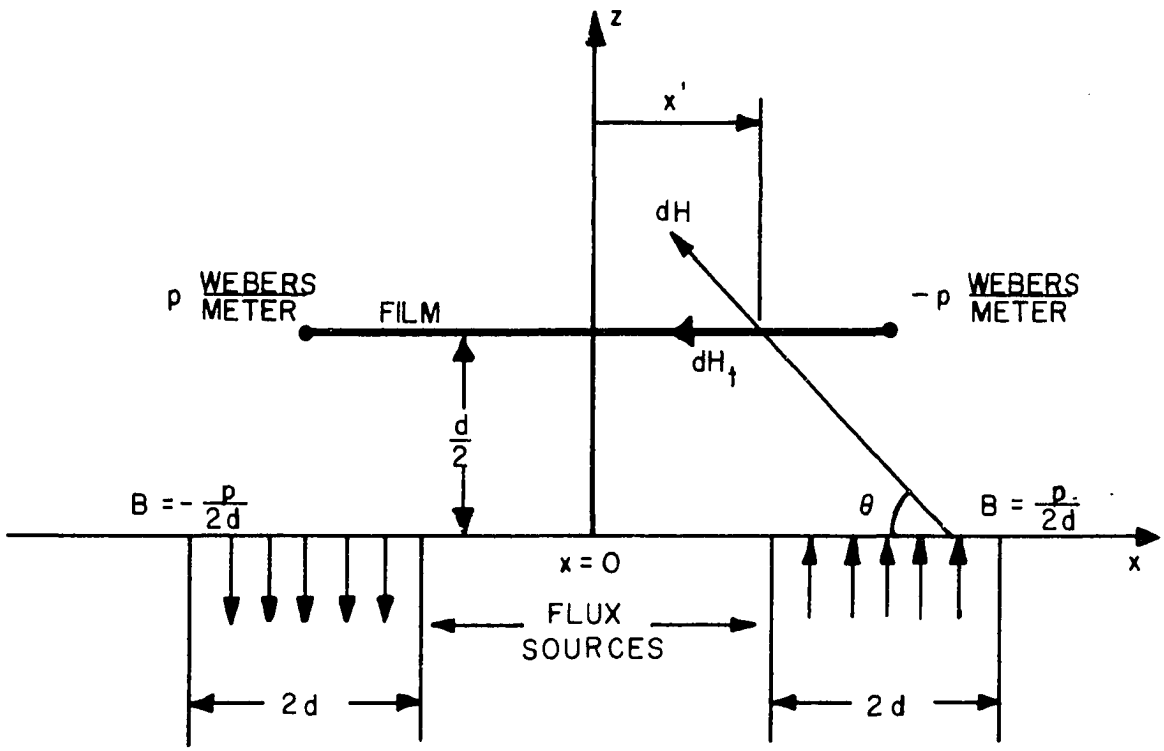


Figure 9. Model for calculation of trapped-flux field

uniform distribution, leading to a source flux density equal to p/2d, where p is once again the linear pole density representing the film edge. It is now necessary to calculate the tangential field in the plane of the film caused by this pair of sources with the film absent. Once again the infinite line pole concept will be used, making the two sources infinite in extent perpendicular to the cross section of the conductor. For the right-hand source,

$$dH = \frac{(p/2d)dx}{2\pi\mu_o r}$$

$$dH_t = dH \sin\theta = \frac{p}{4\pi d\mu_o r} \cdot \frac{x-x'}{r} = \frac{p\,(x - x')}{4\pi d\mu_o[(x-x')^2+(d/2)^2]}$$

$$H_t(x') = \frac{p}{4\pi d\mu_o} \int_{b/2 - d}^{b/2 + d} \frac{(x - x')\,dx}{(x - x')^2 + (d/2)^2}$$

$$= \frac{p}{8\pi d\mu_o} \ln \frac{(b/2 + d - x')^2 + (d/2)^2}{(b/2 - d - x')^2 + (d/2)^2}$$

$$= \frac{p}{8\pi d\mu_o} \ln \frac{(1 + 2d/b - 2x'/b)^2 + (d/b)^2}{(1 - 2d/b - 2x'/b)^2 + (d/b)^2}$$

$$= \frac{p}{8\pi b\mu_o} \frac{b}{d} \ln \frac{(1 + 2d/b - 2x'/b)^2 + (d/b)^2}{(1 - 2d/b - 2x'/b)^2 + (d/b)^2}$$

$$= \frac{p}{8\pi b\mu_o} F(x', d/b) \qquad (63)$$

Because of symmetry, the field due to both sources, denoted by $H_T$, is simply the sum of $H_t$ evaluated at equal-magnitude, opposite-sign values

of the argument x', so that, with p = Mf for a film in a remanent state,

$$H_T = 3.17 \times 10^4 \left(\frac{Mf}{b}\right) [F(x', d/w) + F(-x', d/w)] \qquad (64)$$

This quantity is plotted in Figure 10 for various values of d/b. Also shown in Figure 10 are the average values of each of the curves over the film surface. These average values represent the effective trapped-flux field under the assumption of homogeneous rotation.

It is now possible to calculate the effective torque produced by the trapped-flux field. Refer to Figure 11. The four solid rectangles are the four flux sources under the film edges. A check of the values of $B_s$ given will show that each has the proper value to keep the normal flux density at the conductor surface at its proper value, i.e., zero under the top and bottom edges and Mf/2d and -Mf/2d under the right- and left-hand edges, respectively. The torque caused by these sources is

$$\begin{aligned} T_T &= M_x H_{Ty} - M_y H_{Tx} \\ &= M \cos\theta (H_T \sin\theta) - M \sin\theta (H_T) (\cos\theta - 1) \\ &= MH_T \sin\theta \end{aligned} \qquad (65)$$

This torque, like the eddy-current torque of the previous section, opposes rotation of the magnetization for $0 < \theta < \pi$.

The question arises as to how any voltage may be induced in the sense line if the two crossed conductors repel the flux attempting to penetrate them. Even though this does occur, the conductors are of finite width and the flux simply "wraps around" the sense line. The output voltage will

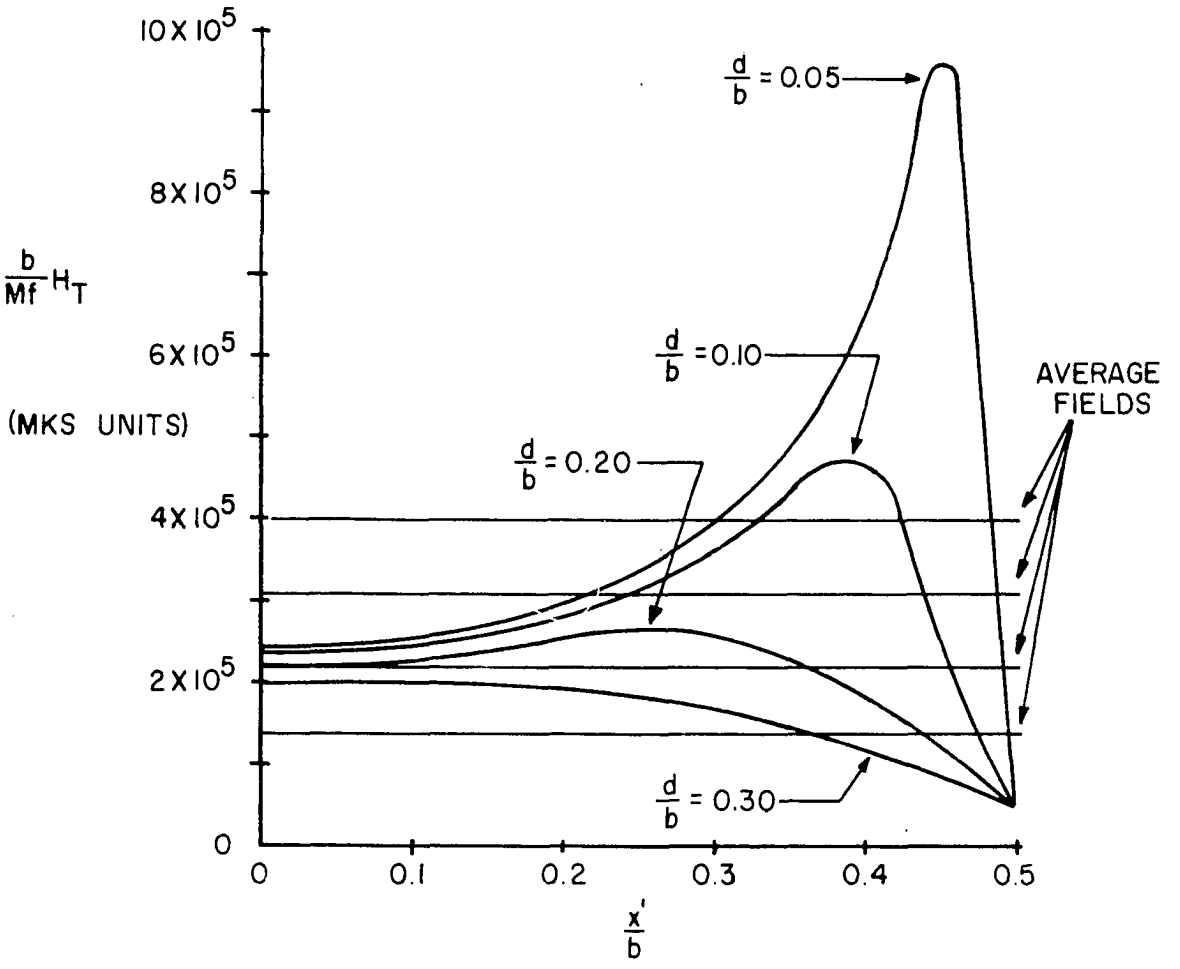


Figure 10. Tangential trapped-flux field in plane of film

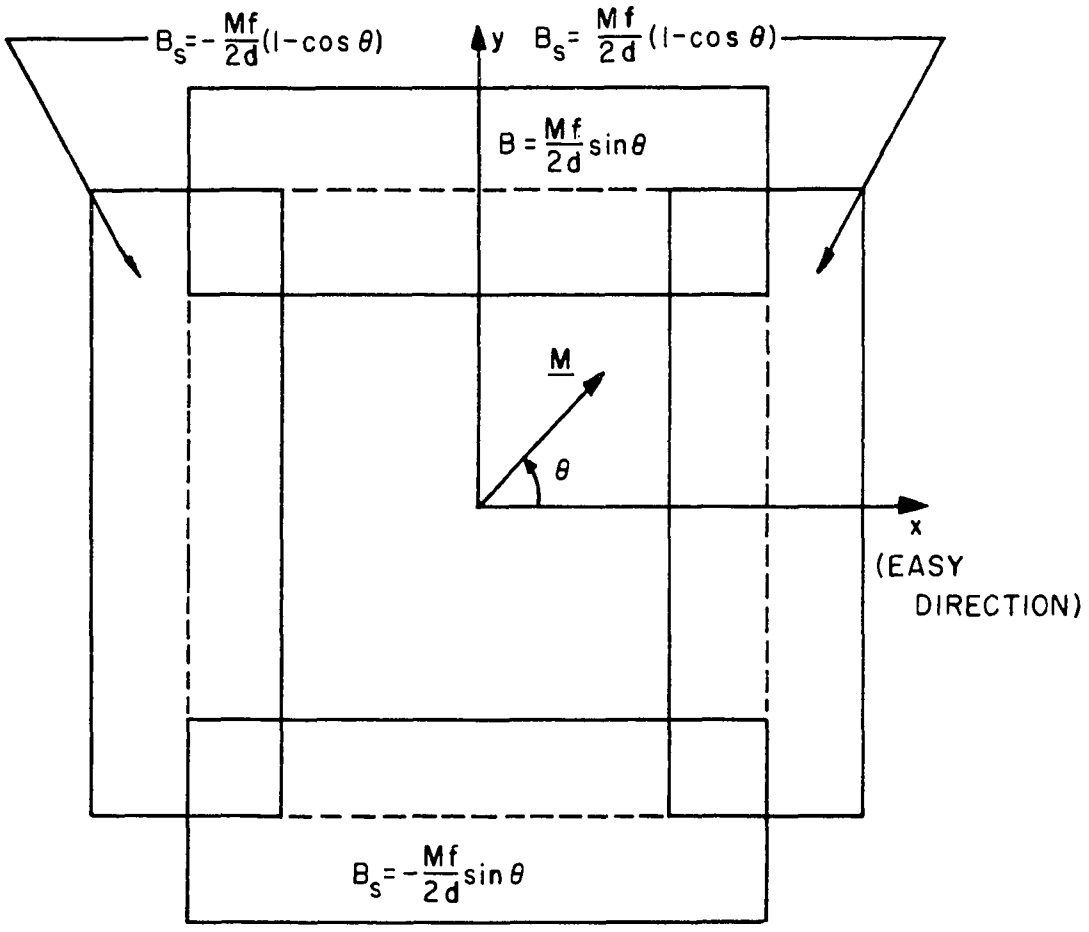


DOTTED LINES INDICATE EFFECTIVE FILM PERIMETER
FLUX SOURCE DENSITIES $B_s$ POSITIVE OUT OF PAPER

Figure 11. Top view of model for trapped-flux torque determination

probably be lessened, however, since some of the flux emanating from a given film edge will terminate on the opposite edge of the same film rather than couple across to the other film because of this distortion in the flux path.

As a sidelight, it is interesting to note that this analysis would be applicable to the study of an inductive non-destructive read-out method such as that proposed by Daughton, Smay, Pohm, and Read (4).

## D. Summary of Analysis

Upon the application of a drive field, the predominant field inhibiting film switching would be the lossless trapped-flux field. If the inductive relaxation time were significantly long, appreciable magnetization rotation could occur before resistive effects become important. Once the film flux has penetrated into the conductor, magnetization rotation would slow down and resistive eddy-current effects would predominate.

Note that the trapped-flux torque $T_T$ given by Equation 65 is zero initially and increases to a maximum of $MH_T$ at $\theta = 90^o$. This means that the film could switch through an appreciable angle $\theta$ before eddy-current effects begin to inhibit rotation. This statement is further supported by noting that $H_T$, the trapped-flux field, is for practical bit geometry, on the order of 100 or 200 ampere-turns/meter, which would probably be somewhat less than the drive field. Thus, unless the conductors are made very thin, probably much less than 0.1 mils, eddy-current damping will play a subordinate role and the trapped-flux field will have only a moderate effect, meaning that the film response will be quite dependent on the rise-time of the line driving source.

# III. EXPERIMENTAL RESULTS

The preceding analysis describes the effects on film switching contributed by the lines coupling the film element. This section will describe attempts made to experimentally verify the analysis. A sample bit was constructed having the following dimensions:

$$b = 25 \text{ mils} = 6.35 \times 10^{-4} \text{ meters} \tag{66}$$

$$c = 0.5 \text{ mils} = 1.27 \times 10^{-5} \text{ meters} \tag{67}$$

$$d = 2 \text{ mils} = 5.08 \times 10^{-5} \text{ meters} \tag{68}$$

The two films were physically about 100 mils square, but, as indicated previously, the effective switching area is determined by the range of the drive field and, for tight coupling, is about equal to the common area of the crossed drive and sense lines, i.e., about 25 mils square. The film was of 80-20 Ni-Fe Permalloy, having a coercive force $H_c$ of about 1.5 oersteds (120 ampere-turns/meter) and an anisotropy field $H_k$ of about 3.5 oersteds (280 ampere-turns/meter). The film thickness f was difficult to determine with the limited equipment available, but was estimated to be about 2000 A ($2 \times 10^{-7}$ meters).

The experimental system is shown schematically in Figure 12. A Tektronix type 110 pulse generator and trigger takeoff system supplies current pulses having rise-times of about 0.35 nanoseconds through a Tektronix type 113 delay cable to the drive line, which is about one centimeter long and shorted at its terminal end to the sandwiching ground planes. Because of this shorted termination and the short line length,

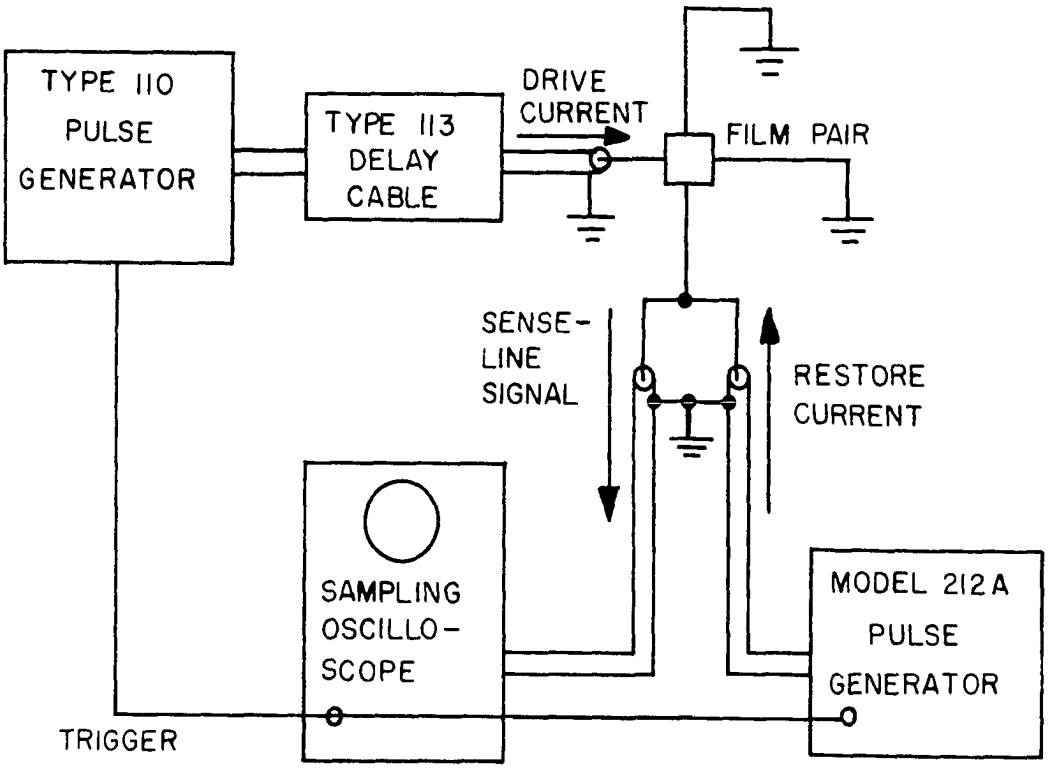


Figure 12. Simplified schematic diagram of experimental system

the actual drive current is about twice the incident current. The sense line signal is displayed on a Tektronix type 543 oscilloscope using a type N plug-in sampling unit having a rise-time of about 0.6 nanoseconds. After each drive pulse a Hewlett-Packard model 212A 50-ohm pulse generator supplies sense-line current pulses of sufficient magnitude and duration to restore the film magnetization vector to its remanent state whose easy direction is parallel to the drive line.

Figures 13 and 14 show oscilloscope photographs of the actual sense-line signals. The lower trace on each photograph of Figure 13 is the sense-line output with no restoring current applied and it indicates the amount of noise present. Figure 13 shows the detail of the low-level portion of the switching waveform, while Figure 14 shows the peak amplitude of the switching signal for drive fields of $H_k$, $2H_k$, $3H_k$, and $4H_k$.

For the particular dimensions given above, Equations 17, 50, and 56 yield the following results:

$$\tau_{max} = 93.5 \text{ nanoseconds} \tag{69}$$

$$R_e = 5.45 \times 10^{-3} \text{ ohms} \tag{70}$$

$$\alpha_e = 4.04 \tag{71}$$

The time constant given by Equation 69 is much longer than the film switching time, and the infinite-relaxation-time calculations are much more applicable than the zero-relaxation-time calculations. Since very little flux penetration occurs during switching, eddy-current losses have little effect, and the only switching field contributed by the presence of the conductors is the trapped-flux field given by Equation 64 and Figure 10.

Figure 13. Sense-line voltage for various drive fields (lower trace shows noise level)

VERTICAL SCALE: 10 MV/CM
HORIZONTAL SCALE: 2 NS/CM

(a) $H_d = H_k$

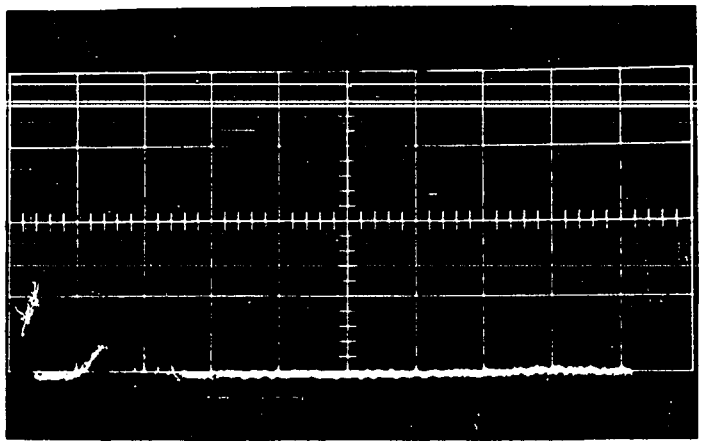

(b) $H_d = 2H_k$

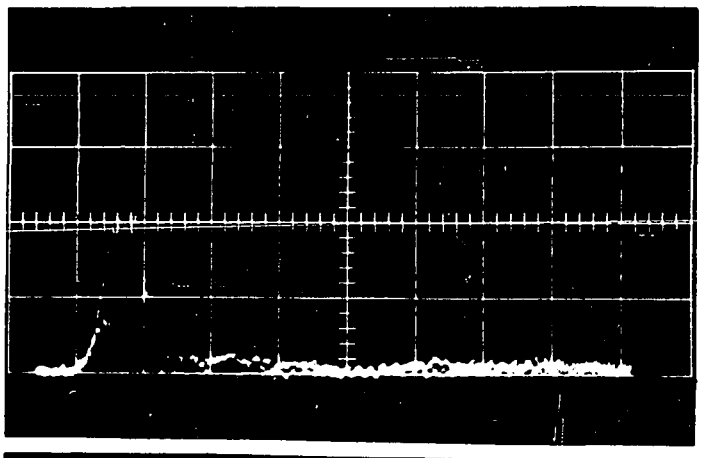

(c) $H_d = 3H_k$

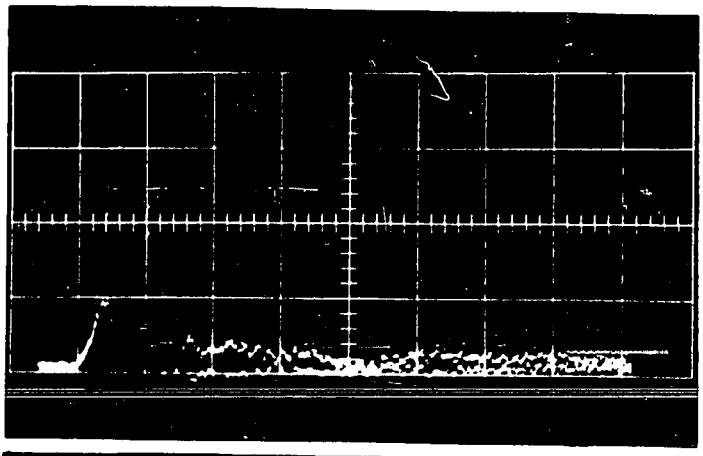

(d) $H_d = 4H_k$

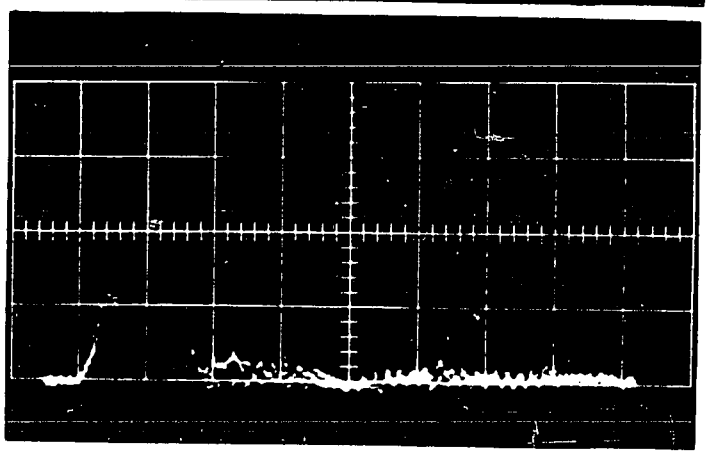

Figure 14. Peak sense-line voltage for $H_d = H_k$, $2H_k$, $3H_k$, $4H_k$

20 MV / CM

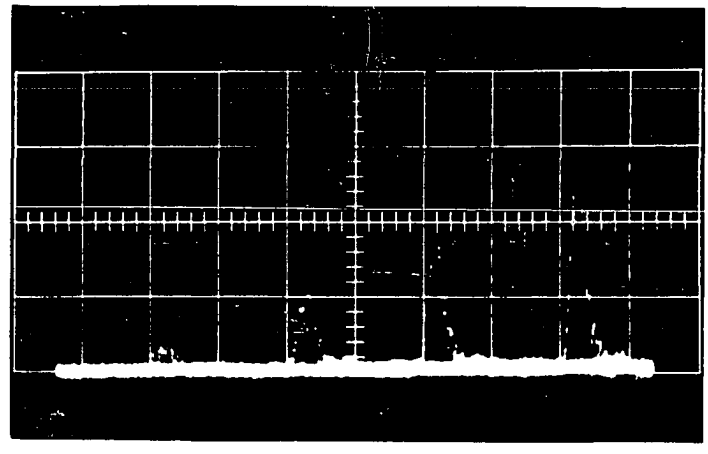

5 NS / CM

The torque produced by this field is given by Equation 65. For the dimensions of the experimental sample, Figure 10 yields approximately

$$(H_T)_{ave} = 96 \text{ ampere-turns/meter} \tag{72}$$

This field adds directly to $H_k$ for small angles of magnetization rotation, explaining the low signal level of Figure 13(a), since this makes the effective $H_k$ about 35 per cent higher than the given value of 280 ampere-turns/meter. This means that the drive field corresponding to Figure 13(a) is large enough to cause magnetization rotation through only a fraction of the predicted value of 90 degrees. In fact, since the trapped-flux torque increases to a maximum at $\theta = 90$ degrees, while the anisotropy torque reaches a maximum at $\theta = 45$ degrees (see Equation 58), the trapped-flux torque has a more profound effect at large values of $\theta$ than does the anisotropy torque.

The switching analysis performed to examine the effects of eddy-current damping is also valid when eddy-current damping is negligible if the eddy-current damping constant $\alpha_e$ is replaced by the phenomenological damping constant $\alpha$, which has a value of about 0.02 for 80-20 Permalloy. The viscous-flow approximation is not as good for such low damping because magnetization precession out of the plane of the film is less negligible, but fair results may be obtained, the error being in the prediction of faster switching times than those physically observed. Dietrich, Proebster, and Wolf (5) show, for example, that experimental switching times for films driven in the hard direction by a drive field $H_d$ equal to 2.35 $H_k$ are about 1.2 nanoseconds, whereas Figure 8 would predict a switching time of about

0.8 nanoseconds. Thus the switching curves given in Figure 8 may be used to predict approximately the switching behavior of a film as it is determined by its own internal damping. For $\alpha = 0.02$, referring to Figure 8,

$$t = \frac{\alpha}{\gamma H_k} t_N = \frac{0.02}{(2.21 \times 10^5)(280)} t_N$$

$$= 0.323\ t_N, \text{ in nanoseconds} \tag{73}$$

$$e_s = \frac{\gamma f M H_k b}{\alpha} e_{sN}$$

$$= \frac{(2.21 \times 10^5)(2 \times 10^{-7})(280)(6.35 \times 10^{-4})}{0.02} e_{sN}$$

$$= 384\ e_{sN}, \text{ in millivolts} \tag{74}$$

Using these values with Figure 8, and making a comparison with Figure 13 and Figure 14, it may be seen that the predicted switching-time values are too low. This is partially due to the error of the viscous-flow approximation, but an even greater error results because the waveforms of Figure 8 do not include the effect of the trapped-flux torque. This torque has negligible effect at small values of $\theta$, but has a very significant effect as $\theta$ becomes large, since, for $\theta$ near 90 degrees, the trapped-flux torque is the only externally-applied torque influencing switching. Thus one would expect the initial portion of the switching waveform to be similar to that predicted by Figure 8 with $\alpha = 0.02$, but the latter portion of the waveform to exhibit the effects of the trapped-flux field, i.e., to be sustained for a substantially longer time than that predicted by Figure 8. This general behavior may be observed in Figures 13 and 14, where the

switching times are about 3 or 4 nanoseconds, and the presence of the trapped-flux field is verified by the long tail on the waveforms, this being especially evident in Figure 13(c).

It would be possible, of course, to add the expression given by Equation 64 for the trapped-flux torque into the expression for the drive torque given by Equation 58, to obtain a new set of torque curves similar to those of Figure 7 and to use these curves to calculate the appropriate switching waveforms. As mentioned before, however, the numerical calculations used to obtain the switching curves of Figure 8 were quite laborious, and the fact that torque curves including the trapped-flux torque would be considerably less linear than those of Figure 7 indicates that the only reasonable way of performing the calculations would be on a digital computer. It is anticipated that this work will be performed, but it will not be included here.

An additional effect not previously considered may also partially account for the fast switching portion of the experimental waveforms. Reference to Figure 10 shows that, for very close film spacing, the trapped-flux field exerts a considerably stronger influence near the film edges than near the center. This means that, for large enough bits, the trapped-flux field may "lock" the portion of the film near the edge, causing the effective film area to break up into edge domains which remain fixed in the presence of the drive field and a central domain whose magnetization may rotate quite freely in the presence of the drive field. It must be emphasized that this will occur only for larger bits, since exchange forces and demagnetizing fields resulting from multiple domain formation

will tend to preserve the single-domain integrity of a smaller bit. A detailed analysis would be necessary to determine the bit size above which this effect would be important, but it is estimated that the 25-mil size used in this experiment is probably right on the borderline. Thus this effect could also account for the initial fast switching. However, since 10-mil bits are considered to be a practical size for memory and logical elements, this effect should be avoidable. Limited fabrication facilities prohibited the use of 10-mil elements in this experiment.

To verify that the zero-relaxation-time analysis is not applicable in this case, the value of $\alpha_e$ given by Equation 71 may be used to compute the unnormalized time and voltage scales in Figure 8 with the result

$$t = \frac{\alpha_e}{\gamma H_k} t_N = \frac{4}{(2.21 \times 10^5)(280)} t_N = 6.49 \times 10^{-8} t_N$$

$$= 64.9\ t_N, \text{ in nanoseconds} \qquad (75)$$

$$e_s = \frac{\gamma f M H_k b}{\alpha_e} e_{sN}$$

$$= \frac{(2.21 \times 10^5)(2 \times 10^{-7})(280)(6.35 \times 10^{-4})}{4.04} e_{sN}$$

$$= 1.97\ e_{sN}, \text{ in millivolts} \qquad (76)$$

Thus the zero-relaxation-time approximation would predict, for $H_d = 4H_k$, for example, a switching time of about 65 nanoseconds and a peak sense-line voltage of about 3 millivolts, whereas the actual measured values given by Figure 13d are about 4 nanoseconds and 80 millivolts, respectively, the discrepancy obviously being quite large. Some discrepancy

is to be expected due to the flux-distribution approximations made, especially the representation of the film edges as concentrated line poles, since the actual pole distribution at the film edges is distributed in such a way as to minimize losses during film switching and will consequently not lead to as concentrated a flux pattern as that assumed. Another slight improvement may be gained by going back to the original equation describing the dynamic behavior of the film, Equation 59, and using a more exact analysis. The Gilbert equation (8) as given by Kikuchi (10) gives a better description of film switching for large damping such as we have here. Appendix C shows that if this equation is used along with the analysis given by Conger and Essig (3) and Olson and Pohm (12), the effective damping constant becomes

$$\alpha_e^1 = \frac{\alpha_e}{\frac{1}{\alpha_e} + \frac{\alpha_e}{(1 + \alpha_e^2)^2}} \tag{77}$$

which, for the value of $\alpha_e$ given by Equation 89, gives

$$\alpha_e^1 = 3.88 \tag{78}$$

This represents only about 4 per cent improvement, however, and the large discrepancy still exists.

The net result of the experimental work is that switching behavior generally consistent with the analysis is observed.

# IV. CONCLUSIONS

1. The coupled-pair bit geometry described in this dissertation appears to have considerable merit when compared to systems now in use. It minimizes such problems as demagnetizing field effects, noise arising from radiation of energy from unshielded lines, and spurious image-current fields. In addition, although not discussed here, it appears to be quite adaptable to mass fabrication, and a study of this problem is now in progress.

2. The fields tending to oppose film switching contributed by the coupling lines must be very carefully classified, i.e., it is important to differentiate between inductive or shielding fields and resistive or eddy-current fields. The two types of fields have markedly different effects on film switching. A problem for further analysis would be to analyze the general case in which both types of fields were considered simultaneously, as opposed to looking only at limiting cases, as was done in this dissertation. The fact that the effects contributed by the conductors are linear inductive and resistive effects should make the general problem amenable to solution even though the film switching behavior itself is quite non-linear.

3. Because the drive field produced by the drive-line current is applied tangentially to the sense line, it will penetrate the sense line relatively fast. For example, the analysis contained in this dissertation indicates that a tangential field applied to a conductor whose thickness is 1/2 mil will have a penetration time constant of about 1.2 nanoseconds, whereas a normally applied flux density, such as that emanating from the

film pair, will have a penetration time constant which is dependent on conductor width as well as thickness. For a 10 mil wide, 1/2 mil thick conductor, the calculated value of this time constant is 37.4 nanoseconds.

4. If coupling lines are fabricated by conventional printed-circuit techniques, implying conductor thickness on the order of 1 mil, the dominant field affecting film switching contributed by the coupling lines will be the inductive trapped-flux field. The relaxation-time analysis given herein may be used to show that, for a 10-mil wide unslotted line, the conductor thickness which will give a relaxation time constant of 1 nanosecond is about 3500 A, implying evaporation fabrication. For conductors this thin, the lossy eddy-current field will evidence itself as viscous damping on the film magnetization, effectively increasing the internal damping constant of the film material, assuming identical drive and sense lines.

5. A well-known method for lessening the effect of coupling lines on film switching is to longitudinally slot these lines. The analysis contained herein should permit a more exact determination of the effects of such slotting than has been heretofore available, minimizing the necessity for the "cut-and-try" method most commonly used. Even though such slotted lines were not explicitly mentioned in the dissertation, the analysis should give quite good results if each separate division of the slotted line is considered individually.

6. The results of the analysis contained herein are valid only if the original assumption of homogeneous rotational switching is valid or nearly so. This assumption will be valid for small bit size, but useful

information would result from a detailed analysis of the effects of bit size on multiple domain formation within the switching element. The results of such an analysis would not only establish the limits of validity for the analysis given here, but would serve as a very useful guide for designers of magnetic film logical and storage systems.

# V. LITERATURE CITED


1. Bittman, E. E. Thin-film memories. Institute of Radio Engineers Transactions on Electronic Computers EC-8: 92-97. 1959.

2. Bradley, E. M. Making reproducible magnetic film memories. Electronics 33, No. 37: 78-81. Sept. 9, 1960.

3. Conger, R. L. and F. C. Essig. Resonance and reversal phenomena in ferromagnetic films. Physical Review 104: 915-923. 1956.

4. Daughton, J. M., T. A. Smay, A. V. Pohm, and A. A. Read. Magnetic film devices using passive loading. Journal of Applied Physics 32S, No. 3: 36S-37S. March 1961.

5. Dietrich, W., W. E. Proebster, and P. Wolf. Nanosecond switching in thin magnetic films. International Business Machines Journal of Research and Development 4: 189-196. 1960.

6. Eggenberger, J. S. Influence of nearby conductors on thin film switching. Journal of Applied Physics 31S, No. 5: 287S-288S. May 1960.

7. Franck, A., G. F. Marette, and B. I. Parsegyan. Deposited magnetic films as logical elements. Eastern Joint Computer Conference Proceedings 16: 28-37. 1959.

8. Gilbert, T. L. A Lagrangian formulation of the gyromagnetic equation of the magnetization field. (Abstract) Physical Review 100: 1243. 1955.

9. Haynes, J. L. Logic circuits using square-loop magnetic devices: a survey. Institute of Radio Engineers Transactions on Electronic Computers EC-10: 191-203. 1961.

10. Kikuchi, R. On the minimum of magnetization reversal time. Journal of Applied Physics 27: 1352-1357. 1956.

11. Landau, L. and E. Lifshitz. On the dispersion of magnetic permeability in ferromagnetic bodies. Physikalische Zeitschrift der Sowjet Union 8: 153-169. 1935.

12. Olson, C. D. and A. V. Pohm. Flux reversal in thin magnetic films of 82% Ni, 18% Fe. Journal of Applied Physics 29: 274-282. 1958.

13. Pohm, A. V. and E. N. Mitchell. Magnetic film memories, a survey. Institute of Radio Engineers Transactions on Electronic Computers EC-9: 308-314. 1960.

14. _____, A. A. Read, R. M. Stewart, Jr., and R. F. Schauer. High-frequency parametrons for computer logic. National Electronics Conference Proceedings 15: 202-214. 1959.

15. _____ and S. M. Rubens. A compact coincident-current memory. Eastern Joint Computer Conference Proceedings 1959: 120-124. 1959.

16. Raffel, J. I. Operating characteristics of a thin film memory. Journal of Applied Physics 30: 78-81. 1960.

17. _____, T. S. Crowther, A. H. Anderson, and T. D. Herndon. Magnetic film memory design. Institute of Radio Engineers Proceedings 49: 155-164. 1961.

18. Read, A. A. Electronic applications of magnetic films. Unpublished Ph.D. thesis. Ames, Iowa, Library, Iowa State University of Science and Technology. 1960.

19. _____ and A. V. Pohm. Magnetic film parametric amplifiers. National Electronics Conference Proceedings 15: 65-78. 1959.

20. Samuels, R. S., and A. A. Read. Thin magnetic film balanced modulators. Unpublished paper presented at the Institute of Radio Engineers Professional Group on Military Electronics winter meeting, Los Angeles, California, Feb. 3-5, 1960. Mimeo. Ames, Iowa, Iowa State University of Science and Technology, Department of Electrical Engineering. ca. 1960.

21. Schauer, R. F., R. M. Stewart, Jr., A. V. Pohm, and A. A. Read. Some applications of magnetic film parametrons as logical devices. Institute of Radio Engineers Transactions on Electronic Computers EC-9: 315-320. 1960.

22. Smith, D. O. Static and dynamic behavior of thin permalloy films. Journal of Applied Physics 29: 264-273. 1958.

## VI. ACKNOWLEDGEMENTS

The author wishes to acknowledge a very deep debt of gratitude to his major professor, Dr. A. V. Pohm, for suggesting the problem and providing many suggestions, much encouragement, and infinite patience. Thanks are also due to many other members of the academic staff at Iowa State University, and to Mrs. Howard Zembsch who typed the manuscript.

# VII. APPENDIX A

## Coupling Factor of Film Coupled Pair

If, in Figure 3, both pairs of infinite line poles are used to calculate $B_T$, the result is

$$B_T = \frac{pd}{2\pi} \left[ \frac{1}{x^2 + (\frac{d}{2})^2} - \frac{1}{(x - b)^2 + (\frac{d}{2})^2} \right] \tag{79}$$

The flux $\phi$ penetrating the center half-plane given by $x < b/2$ is the flux coupling the two adjacent poles at $x = 0$.

$$\phi = b \int_{-\infty}^{b/2} B_T \, dx = \frac{pbd}{2\pi} \left[ \int_{-\infty}^{b/2} \frac{dx}{x^2 + (\frac{d}{2})^2} - \int_{-\infty}^{b/2} \frac{dx}{(x-b)^2 + (\frac{d}{2})^2} \right]$$

$$= \frac{pbd}{2\pi} \left[ \int_{-\infty}^{b/2} \frac{dx}{x^2 + (\frac{d}{2})^2} - \int_{-\infty}^{-b/2} \frac{du}{u^2 + (\frac{d}{2})^2} \right]$$

$$= \frac{pb}{\pi} \left[ \tan^{-1} \frac{b}{d} + \frac{\pi}{2} + \tan^{-1} \frac{b}{d} - \frac{\pi}{2} \right]$$

$$= \frac{2pb}{\pi} \tan^{-1} \frac{b}{d} \tag{80}$$

The ratio of $\phi$ to pb is the ratio of the flux coupling between adjacent poles to that emanating from either of these poles and will be defined as the coupling factor C.

$$C = \frac{\phi}{pb} = \frac{2}{\pi} \tan^{-1} \frac{b}{d} \tag{81}$$

C is plotted in Figure 15 as a function of spacing-to-length ratio $\frac{d}{b}$.

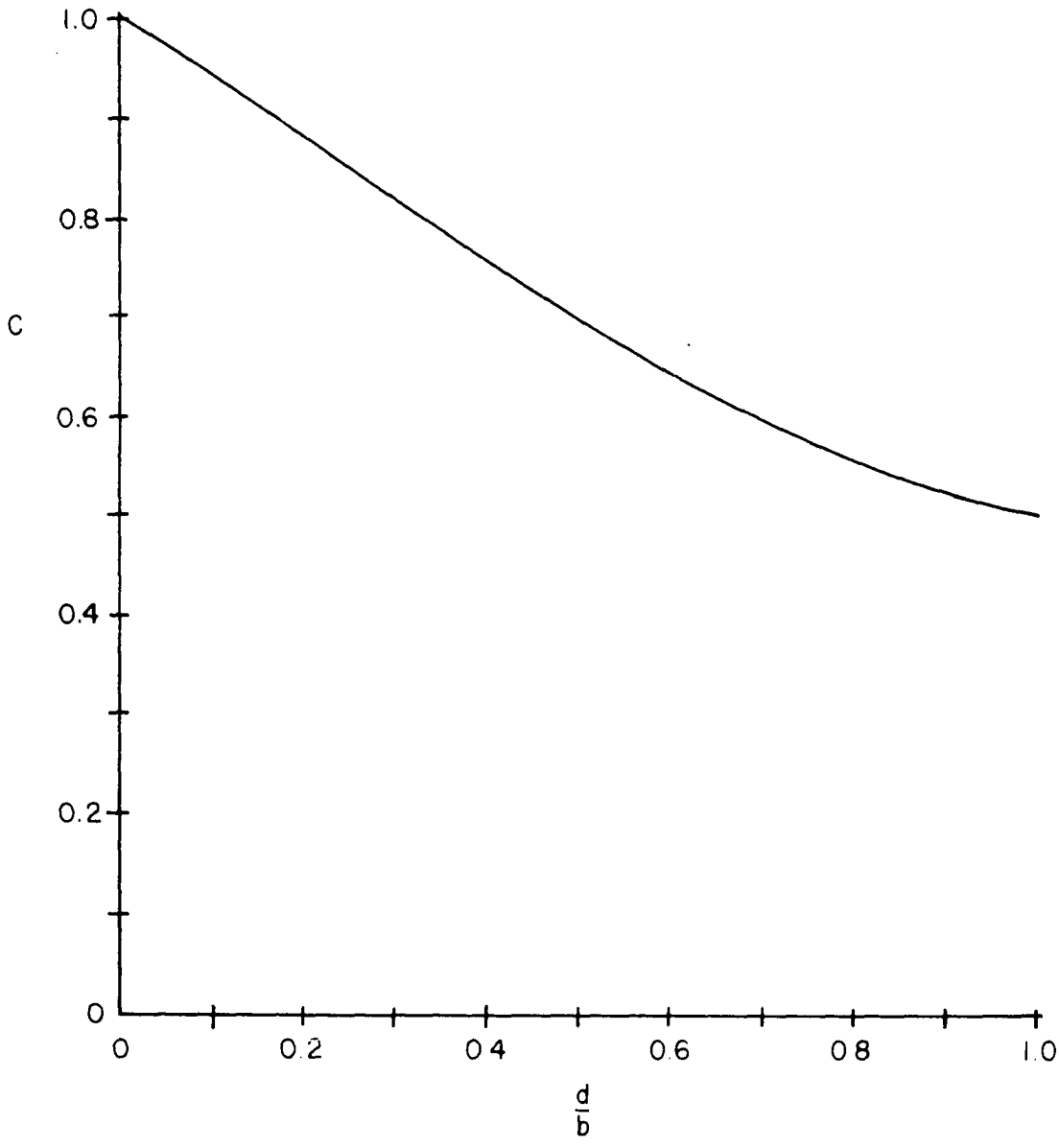


Figure 15. Film-pair coupling factor C versus spacing-to-length ratio

# VIII. APPENDIX B

## Determination of $k_1$ and $k_2$

In Figure 5, let $I_1$ be the current flowing within the conductor across the half-plane given by $x = 0$, $y > 0$.

$$I_1 = c\int_0^{b/2} i_{x1}\Big|_{x=0} dy = \frac{4ck_2\sigma K_a}{\pi}\sum_m \frac{\exp(-\frac{m\pi a}{2b})}{m}\,\mathrm{Sin}\,\frac{m\pi}{2}\int_0^{b/2}\mathrm{Sin}\,\frac{m\pi y}{b}\,dy + k_1\sigma B_o(0)\int_0^{b/2} y\,dy$$

$$= \frac{4ck_2\sigma K_a b}{\pi^2}\sum_m \frac{\exp(-\frac{m\pi a}{2b})}{m^2}\,\mathrm{Sin}\,\frac{m\pi}{2} + k_1\sigma B_o(0)(\frac{b^2}{8}) \qquad (82)$$

Let $I_2$ be the current flowing within the conductor across the half-plane given by $y = 0$, $x > 0$.

$$I_2 = c\int_0^{\infty} i_y\Big|_{y=0} dx = c\Big[\int_0^{a/2} i_{y1}\Big|_{y=0} dx + \int_{a/2}^{\infty} i_{y2}\Big|_{y=0} dx\Big]$$

$$c\int_0^{a/2} i_{y1}\Big|_{y=0} dx = \frac{4k_2c\sigma K_a}{\pi}\sum_m \frac{\exp(-\frac{m\pi a}{2b})}{m}\,\mathrm{Sin}\,\frac{m\pi}{2}\int_0^{a/2}\mathrm{Sinh}\,\frac{m\pi x}{b}\,dx - k_2\sigma c\int_0^{a/2}\int_0^{x} B_o(x)dxdx$$

$$= \frac{4k_2cb\sigma K_a}{\pi^2}\sum_m \frac{\exp(-\frac{m\pi a}{2b})}{m^2}\,\mathrm{Sin}\,\frac{m\pi}{2}\,(\mathrm{Cosh}\,\frac{m\pi a}{2b} - 1) - k_2\sigma c\int_0^{a/2}\int_0^{x} B_o(x)dxdx \qquad (83)$$

$$c\int_{a/2}^{\infty} i_{y2}\Big|_{y=0} dx = \frac{4k_2 c\sigma K_a}{\pi} \sum_m (-\frac{1}{m})\text{Cosh } \frac{m\pi a}{2b} \text{ Sin } \frac{m\pi}{2} \int_{a/2}^{\infty} \exp\ (-\frac{m\pi x}{b})\, dx$$

$$= \frac{-4k_2 cb\sigma K_a}{\pi^2} \sum_m \frac{1}{m^2} \text{ Cosh } \frac{m\pi a}{2b} \text{ Sin } \frac{m\pi}{2} \exp\ (-\frac{m\pi a}{2b}) \qquad (84)$$

Continuity requires that $I_1 = -I_2$. Plugging Equations 82, 83, and 84 into this relationship gives

$$k_1 B_o(0)(\frac{b^2}{8}) = k_2 \int_o^{a/2} \int_o^x B_o(x)dx \qquad (85)$$

Employing the relationship given by Equation 24 for $B_o(x)$, we obtain

$$k_1(\frac{2p}{a\Delta T})(\frac{b^2}{8}) = k_2 \int_o^{a/2} \int_o^x \frac{2p}{a\Delta T} \text{Cos}^2 \frac{\pi x}{a}\, dx$$

$$= \frac{k_2 pa}{\Delta T} [\ \frac{1}{8} + \frac{1}{2\pi^2}] \qquad (86)$$

from which

$$\frac{k_1}{k_2} = 0.702\ (\frac{a}{b})^2 \qquad (87)$$

Combining this with Equation 32 gives

$$k_1 = \frac{0.702}{(\frac{b}{a})^2 + 0.702} \qquad (88)$$

$$k_2 = \frac{(\frac{b}{a})^2}{(\frac{b}{a})^2 + 0.702} \qquad (89)$$

# IX. APPENDIX C

## Summary of Switching Analysis Using the Gilbert Modification of the Landau-Lifshitz Equation

The most commonly used equation for describing the dynamic behavior of the magnetization vector $\underline{M}$ in thin magnetic films is due to Landau and Lifshitz (11) and may be written as

$$\dot{\underline{M}} = \gamma(\underline{M} \times \underline{H}) - \frac{\alpha\gamma}{M} \underline{M} \times (\underline{M} \times \underline{H}) \tag{90}$$

where $\gamma$ is the gyromagnetic ratio, $\alpha$ is a phenomenological damping constant, and $\underline{H}$ is the effective magnetic field. Gilbert (8) suggested a modification of this equation in which the damping appears more naturally in direct proportion to $\underline{M}$, and Kikuchi (10) gives the modified equation as

$$\dot{\underline{M}} = \gamma\underline{M} \times (\underline{H} - \frac{\alpha}{\gamma M} \dot{\underline{M}}) \tag{91}$$

Application of vector identities reduces this equation to

$$\dot{\underline{M}} = \frac{\gamma}{1 + \alpha^2} (\underline{M} \times \underline{H}) - \frac{\alpha\gamma}{1 + \alpha^2} [\underline{M} \times (\underline{M} \times \underline{H})] \tag{92}$$

This equation is more satisfactory than Equation 90 since it exhibits proper behavior for large $\alpha$, as Equation 90 does not. Since for 80-20 Ni-Fe Permalloy $\alpha$ is about equal to 0.02, Equation 90 and Equation 92 becomes essentially identical for this material. However, for the eddy-current damping described in this dissertation, the two equations are quite dissimilar and special precautions must be taken.

Reference to Equation 56 shows that the torque produced by eddy-current fields is viscous in nature. This torque may thus be represented

by an effective field proportional to $\theta$ and to M, this field being of the same type given by the second term in brackets in Equation 91. Thus, if $\alpha_e$, the dimensionless eddy-current damping constant defined by Equation 56, is inserted in Equations 91 and 92 in place of $\alpha$, these equations should describe the dynamic behavior of the magnetization.

Olson and Pohm (12), partially using the analysis of Conger and Essig (3), give a solution of Equation 90 for planar permalloy films as follows:

$$\theta = \frac{\gamma}{M}\left(\frac{1}{\alpha} + \alpha\right) T_d(\theta) \tag{93}$$

where $T_d$ is the drive torque given by Equation 58. Note that Equation 92 is exactly the same as Equation 90 except that $\alpha$ is replaced by $\alpha/1 + \alpha^2$ and $\gamma$ is replaced by $\gamma/1 + \alpha^2$. Equation 93 should thus give a solution to Equation 92 if these substitutions are made. Replacing $\alpha$ by $\alpha_e$,

$$\theta = \frac{\gamma}{(1 + \alpha_e^{\,2})M}\left[\frac{1 + \alpha_e^{\,2}}{\alpha_e} + \frac{\alpha_e}{1 + \alpha_e^{\,2}}\right] T_d(\theta)$$

$$= \frac{\gamma}{M}\left[\frac{1}{\alpha_e} + \frac{\alpha_e}{(1 + \alpha_e^{\,2})^2}\right] T_d(\theta) \tag{94}$$

Equation 94 is equivalent to Equation 59, where the explicit form for $T_d$ has been inserted into Equation 59. If we denote by $\alpha_e^1$ the equivalent damping constant which Equation 94 tells us must replace $\alpha_e$ in Equation 59, we obtain

$$\alpha_e^1 = \frac{1}{\frac{1}{\alpha_e} + \frac{\alpha_e}{(1 + \alpha_e^{\,2})^2}} \tag{95}$$